

1 **PIWIL2 downregulation in colon cancer promotes transposon activity and pro-tumorigenic**  
2 **phenotypes**

3  
4 **Authors:**

5 Alyssa Risner<sup>1</sup>, Joyce Nair-Menon<sup>1</sup>, Abhinav Cheedipudi<sup>2</sup>, Joe R Delaney<sup>3</sup>, Vamsi Gangaraju<sup>3</sup>,  
6 Antonis Kourtidis<sup>1</sup>

7 **Affiliations**

8 <sup>1</sup>Department of Regenerative Medicine and Cell Biology, Medical University South Carolina,  
9 Charleston, SC

10 <sup>2</sup>University of South Carolina, Columbia, SC.

11 <sup>3</sup>Department of Biochemistry and Molecular Biology, Medical University South Carolina, Charleston,  
12 SC

13  
14 Corresponding author: Antonis Kourtidis, [kourtidi@musc.edu](mailto:kourtidi@musc.edu)

15

16 **ABSTRACT**

17 Reactivation of transposable elements (TEs) in somatic tissues, particularly of LINE-1, is associated  
18 with disease by causing gene mutations and DNA damage. Previous work has shown that the PIWI  
19 pathway is crucial for TE suppression in the germline. However, the status and function of this pathway  
20 has not been well characterized in differentiated somatic cells and there is lack of consensus on the  
21 role of the pathway in somatic tumorigenesis. To shed light on this conundrum, we examined the PIWI  
22 pathway in colon cancer through a combination of bioinformatic analyses and cell-based assays.  
23 Shifted Weighted Annotation Network (SWAN) analysis revealed that the pathway experiences  
24 significant allelic losses in colon cancer and that PIWIL2, the main catalytic component of the pathway  
25 responsible for TE silencing, experiences the highest percent deletions. PIWIL2 is downregulated in  
26 colon tumors of advanced stage, nodal metastasis, and in certain subtypes, correlating with poor  
27 survival, while it is even downregulated in ulcerative colitis, an inflammatory bowel disease that  
28 predisposes to colon cancer. Knockout studies in colon epithelial Caco2 cells show that PIWIL2  
29 depletion leads to increased anchorage-independent growth, increased LINE-1 levels and activity, and  
30 in DNA damage, altogether highlighting a tumor-suppressing role of PIWIL2 in the colon.

31

32 **SUMMARY STATEMENT**

33 This study investigates the PIWI-piRNA pathway in colon cancer using a nuanced bioinformatic and  
34 cell-based approach, linking the downregulation of PIWIL2 to disease progression, transposable  
35 element activation and DNA damage.

## 36 INTRODUCTION

37 Transposons, or transposable elements (TEs), are mobile DNA elements that make up approximately  
38 45% of the human genome. Although they have been primarily studied in the germline and are overall  
39 considered inactive in differentiated somatic epithelial tissues, their reactivation has been shown to lead  
40 to a variety of diseases through the introduction of regulatory or protein coding changes when integrated  
41 into a new site (Beck et al., 2011, Elbarbary et al., 2016, Hancks and Kazazian, 2016). Additionally,  
42 recent studies have demonstrated that genomic instability, oncogene expression, and high mutation  
43 rates in approximately 50% of tumors are linked to increased TE activity (Tubio et al., 2014, Jang et al.,  
44 2019).

45 Among the several TE families existing in the human genome, the Long Interspersed Nuclear Element-  
46 1 (LINE-1) is the most abundant and the only autonomously mobilizing TE family in humans (Beck et  
47 al., 2011). While most copies of the LINE-1 TE are inactive due to truncations and mutations, 100-150  
48 copies are functionally active in disease (Wang et al., 2024, Beck et al., 2010, Tubio et al., 2014,  
49 Rodriguez-Martin et al., 2020). The functional LINE-1 copies contain protein-coding open reading  
50 frames (ORFs), ORF1 and ORF2, that encode an RNA-binding protein and reverse transcriptase,  
51 respectively, to facilitate reverse transcription of the LINE1 RNA transcript (Beck et al., 2011, Elbarbary  
52 et al., 2016, Hancks and Kazazian, 2016). Reactivation of LINE-1 has been frequently observed in  
53 somatic tissues and particularly in the gastrointestinal tract, where it has been associated with colon  
54 cancer, the second most frequent and third deadliest cancer type in both sexes (Pitkanen et al., 2014,  
55 Solyom et al., 2012, Ewing et al., 2015, Tubio et al., 2014, Zhuo et al., 2015, Nam et al., 2023, Siegel  
56 et al., 2024). Indeed, recurrent LINE-1 insertions have been identified to cause mutations in known  
57 oncogenes or tumor suppressors such as APC, a key initiating event in colorectal tumorigenesis,  
58 indicating that LINE-1 retro-transposition events have the ability to serve as tumor-initiating events in  
59 colon cancer (Cajuso et al., 2019, Scott et al., 2016, Miki et al., 1992). In fact, colon tumors are  
60 significantly enriched with somatic retro-transpositions (Rodriguez-Martin et al., 2020). However, the  
61 reasons for increased TE activity in these tumors are still poorly understood.

62 Mechanisms of TE regulation previously described in the germline include DNA methylation and histone  
63 modifications of LINE-1 loci, as well as RNA interference by small RNAs through the PIWI  
64 pathway (Kuramochi-Miyagawa et al., 2008, Sigurdsson et al., 2012, Ariumi, 2016, Berrens et al., 2017,  
65 Walter et al., 2016). The PIWI pathway was first described in *Drosophila* to suppress TEs in the germline  
66 and to be required for spermatogenesis (Ku and Lin, 2014). PIWI proteins are members of the Argonaute  
67 family of endoribonucleases that bind PIWI interacting RNAs (piRNAs), a distinct class of small non-  
68 coding RNAs that are 24-32 nucleotides in length, altogether forming the piRNA-induced silencing  
69 complex (piRISC) (Siomi et al., 2011). Most piRNAs are derived from piRNA clusters within the genome,

70 which are also locations of a large number of truncated TEs (Siomi et al., 2011). piRISC recognizes  
71 piRNA - complementary RNA transcripts of TEs in their cytosolic phase and cleaves them, subsequently  
72 preventing retro-transposition and DNA mutagenesis (Ramat and Simonelig, 2021, Watanabe and Lin,  
73 2014, Weick and Miska, 2014).

74 The PIWI-piRNA mechanism is conserved throughout evolution, including in mammals, where it has  
75 been found to be required for germline maintenance in mice (Unhavaithaya et al., 2009, Sun et al.,  
76 2022, Kuramochi-Miyagawa et al., 2008, Li et al., 2021). In humans, there are four PIWI protein  
77 members, namely PIWIL1, PIWIL2, PIWIL3 and PIWIL4 (Zeng et al., 2020). In addition to PIWI proteins,  
78 the TE targeting function of piRISC is enabled by a number of additional protein components, including  
79 the Tudor family of proteins that act as protein scaffolds, as well as by RNA helicases, such as  
80 MOV10L1 and DDX4 (Siomi et al., 2010, Mathioudakis et al., 2012, Reuter et al., 2009, Gao et al., 2024,  
81 Frost et al., 2010, Vourekas et al., 2015, Fu et al., 2019, Li et al., 2021, Wenda et al., 2017). Although  
82 it was previously thought that PIWI proteins were germline - specific in humans, a recent study that  
83 sought to characterize their expression patterns across multiple tissue types showed that PIWI proteins,  
84 namely PIWIL2 and PIWIL4, are also expressed substantially in somatic tissues (Meseure et al., 2020).

85 In addition to their expression in normal somatic tissues, a number of studies have suggested that PIWI  
86 proteins are overexpressed in somatic tumors and act as oncogenes, in a similar fashion to the overall  
87 scheme of re-expression of stem cell and germline markers in tumors; however, other studies have  
88 shown that PIWI proteins in fact act as tumor suppressors, altogether exposing a lack of consensus on  
89 the function of PIWI proteins in somatic tissues and tumors (Lee et al., 2006, Lu et al., 2012, Wang et  
90 al., 2015, Zeng et al., 2017, Eckstein et al., 2018, Meseure et al., 2020, Kishani Farahani et al., 2023,  
91 Shi et al., 2020). This is particularly the case for PIWIL2, which is the key endoribonuclease that binds  
92 primary piRNAs in piRISC to target TE RNA transcripts for degradation, including LINE-1 (Siomi and  
93 Siomi, 2015, De Fazio et al., 2011). Still, the function of PIWIL2 in differentiated epithelial tissues and  
94 its role in tumorigenesis has not been well characterized (Yan et al., 2011, Ross et al., 2014b, Peng and  
95 Lin, 2013, Martinez et al., 2015, Jacobs et al., 2016, Gao, 2008, He et al., 2010, Liu et al., 2010).  
96 Previous *in vitro* work studying PIWIL2 has been primarily conducted in transformed cancer cell lines,  
97 or in commonly used cell lines such as HEK-293 cells, none of which are representative of the normal  
98 differentiated epithelium. Here, we aimed to elucidate the expression and function of the PIWI complex  
99 in colon cancer, through performing bioinformatic analyses and functional assays in colon epithelial  
100 cells.

## 102 RESULTS

## SWAN analysis identifies dysregulation of the PIWI pathway in colon cancer

To decipher the expression and role of the PIWI-piRNA pathway in colon cancer, we first used bioinformatic tools to investigate the status of key proteins of the pathway through mining data from The Cancer Genome Atlas (TCGA). To do this, we used the Shifted Weighted Annotation Network (SWAN) algorithm, which has the capability to interrogate pathway and copy-number alterations (CNAs) within the TCGA data set (Bowers et al., 2022). Networks in the algorithm are scored based on the number of interactions within the pathway and if haploinsufficiency data are available for the dataset. The Single-pathway SWAN algorithm was used to perform Gene Ontology Biological Process Analysis on the PIWI-piRNA metabolic pathway in the TCGA colon adenocarcinoma (COAD) dataset (**Fig 1**). The pathway was scored by the SWAN algorithm as overall haploinsufficient (**Fig 1A**). Allelic losses or gains were then mapped to each respective chromosome by the algorithm (**Fig 1B**). This analysis showed that there is not a single “hot spot” across the genome where all the observed allelic losses or gains are concentrated, but that these are dispersed throughout the genome. Notably, PIWIL2, which is the main catalytic component of the primary piRNA pathway involved in TE regulation, experienced the highest percent deletion and allelic losses of the pathway queried (**Fig 1C**). PIWIL1 and PIWIL4 were not significantly enriched in the SWAN algorithm with gains or losses, and PIWIL3 was excluded from the pathway by the algorithm. Proteins required for both primary and secondary piRNA processing experienced allelic losses, including the nuclease EXD1; RNA helicase DDX4 (*Vasa* in *Drosophila*; *MVH* in mice); PLD6 (*Zucchini* in *Drosophila*; *mitoPLD* in mice) that generates the 5' end of primary piRNAs; RNA helicase MOV10L1 that is required for stabilizing the primary piRNA transcript; as well as TDRD1 and TDRD9 that are required for stabilization of the complex and piRNA loading (Yang et al., 2016, Wenda et al., 2017, Nishimasu et al., 2012, Han et al., 2015, Vourekas et al., 2015, Zhang et al., 2019, Mathioudakis et al., 2012). Interestingly, four components of the pathway experienced high percentages of allelic amplifications and allelic gains in the COAD dataset, including TDRD12, TDRKH, ASZ1 and FKBP6. TDRD12 is a binding partner of EXD1 while TDRKH is required for 3' end processing of piRNAs (Pandey et al., 2013, Saxe et al., 2013). ASZ1 is required for phased piRNA biogenesis through the stabilization of PIWIL2 and PIWIL4, while FKBP6 is a co-chaperone to facilitate piRNA loading (Ma et al., 2009, Ikeda et al., 2022, Saxe et al., 2013, Xiol et al., 2012). Furthermore, we queried whether PIWIL2 allelic loss correlates with patient survival using the cBioportal copy number alteration (CNA) tool; indeed allelic loss of PIWIL2 correlates with poorer patient survival compared to patients without an allelic loss (**Fig 1D**). The results from the SWAN and cBioportal analyses highlight the overall loss of regulation of the entire piRNA biogenesis pathway in colon cancer and identify PIWIL2 as a top candidate for the loss of pathway's regulation.

## PIWIL2 is downregulated in colon cancer in correlation with disease progression

138 Next, we queried PIWIL2 expression levels in the TCGA dataset using the University of Alabama at  
139 Birmingham CANcer data analysis portal (UALCAN) (**Fig 2, Fig 3**). A general overview of PIWIL2  
140 expression among all tissues and cancers included in the database confirms the high expression of  
141 PIWIL2 in normal tissues particularly of gastrointestinal origin, namely colon, rectal, and gastric (**Fig 2**).  
142 We then interrogated the COAD (colon adenocarcinoma) dataset to examine PIWIL2 mRNA expression  
143 stratified by normal vs: primary tumor; tumor stages; nodal metastasis; p53 status; histological subtype  
144 (adenocarcinoma, mucinous adenocarcinoma); microsatellite stability; age; weight; race; and biological  
145 sex (**Fig 3A-J**). Comparisons between normal and primary tumors showed decreased PIWIL2 levels in  
146 tumors, as well as when tumors were stratified by stage I-IV (**Fig 3A,B**). Due to high variance in  
147 expression, this downregulation of PIWIL2 only reached statistical significance in the transition to stage  
148 IV (**Fig 3B**); however, downregulation of PIWIL2 in tumors was significant when the tumors were  
149 stratified by lymph node metastasis, particularly in N0 tumors compared to normal and between N0 and  
150 N2 tumors, denoting correlation of PIWIL2 both with early transformation at N0 and with tumor  
151 aggressiveness at N2 (**Fig 3C**). Interestingly, PIWIL2 downregulation does not correlate with p53 status  
152 (**Fig 3D**); however, PIWIL2 was significantly downregulated in adenocarcinomas compared to normal  
153 tissues, and even more downregulated in mucinous adenocarcinomas (**Fig 3E**). Mucinous  
154 adenocarcinomas possess a high degree of microsatellite instability, which is a feature that is used to  
155 categorize colon tumors in MSI-H (microsatellite instability - high), MSI-L (microsatellite instability - low),  
156 and MSS (microsatellite stable). Since the UALCAN database does not include the option of stratifying  
157 tumors based on microsatellite instability, we used GEPIA2(Tang et al., 2019) to examine expression  
158 of PIWIL2 in these sub-categories of tumors. Interestingly, PIWIL2 is downregulated in MSI-L tumors  
159 and even more significantly in MSI-H tumors, compared to MSS tumors (**Fig. 3F**). This result is in  
160 agreement with the downregulation of PIWIL2 in the mucinous adenocarcinomas, which are  
161 microsatellite unstable. PIWIL2 also seems to be progressively downregulated by age, where MSI-H  
162 tumors are also more prevalent (Guidoboni et al., 2001) (**Fig 3G**). Finally, there were no statistically  
163 significant differences in PIWIL2 expression by weight, race, or biological sex (**Fig 3H,I,J**). Low PIWIL2  
164 expression in colon tumors was also correlated with poor patient survival among all tumor stages, when  
165 stratified by stages 1-3 combined, and even more pronounced in stage 4, using the Kaplan-Meier  
166 Plotter web-based tool (**Fig 3K-M**), which is in agreement with the CNA data (**Fig 1D**).

167  
168 Furthermore, examination of the methylation levels of the PIWIL2 promoter using UALCAN showed  
169 that this was significantly elevated in colon tumors overall, indicated by a higher methylation beta-value,  
170 as well as when these tumors were stratified by stage, nodal metastasis; p53 status; histological  
171 subtype; age; biological sex; weight; and race (**Fig 4**). These findings indicate that PIWIL2 expression  
172 is suppressed across colon cancer due, in part, to promoter methylation and microsatellite instability.

173

## 174 **PIWIL2 is also downregulated in ulcerative colitis**

175 Since we identified downregulation of PIWIL2 in colon tumors beginning from early forms of the disease,  
176 such as in N0 tumors, we then sought to examine the status of PIWIL2 in precancerous conditions in  
177 the colon, such as in inflammatory bowel disease that significantly increases the risk for colon  
178 cancer(Kim and Chang, 2014, Gordon et al., 2018). To do this, we examined the expression levels of  
179 members of the PIWI pathway that we identified using the SWAN analysis, using expression data from  
180 patients with ulcerative colitis, one of the main manifestations of inflammatory bowel disease, available  
181 through the PreMedIBD database(Linggi et al., 2021). This analysis showed that out of all the members  
182 of the PIWI-piRNA pathway that were queried, PIWIL2 was the gene that was more predominantly  
183 downregulated in ulcerative colitis (**Fig 5**). This further denotes PIWIL2 as the member of the pathway  
184 that is potentially most critical for tumor initiation. Altogether, the above analyses demonstrate that the  
185 PIWI pathway is dysregulated in colon cancer, particularly its main component PIWIL2, and its  
186 downregulation correlates with disease initiation and progression.

187

## 188 **PIWIL2 depletion in colon epithelial cells promotes pro-tumorigenic behavior**

189 Given that PIWIL2 exhibits the most allelic losses in the entire PIWI pathway and is also downregulated  
190 in ulcerative colitis and colon cancer correlating with disease progression (**Fig 1C, Fig 3, Fig 4, Fig 5**),  
191 we sought to investigate whether loss of PIWIL2 may indeed promote pro-tumorigenic phenotypes. To  
192 do this, we used Caco2 colon epithelial cells, a broadly used in vitro model of the well-differentiated  
193 colonic epithelium(Grasset et al., 1984, Hidalgo et al., 1989, Sambuy et al., 2005). We first confirmed  
194 that PIWI proteins were expressed in these cells, by examining our publicly available RNA-sequencing  
195 data(Daulagala et al., 2024). The data confirmed expression of PIWIL2 and PIWIL4 in Caco2 cells, but  
196 not of PIWIL1 and PIWIL3 (**Supplemental Table 1**). We then generated a PIWIL2 CRISPR/Cas9  
197 mediated knockout (KO) in Caco2 cells. The PIWIL2 KO was overall not well tolerated by these cells,  
198 since most cells didn't survive selection; however, we isolated cells where we confirmed 50%  
199 downregulation of PIWIL2 by qRT-PCR (**Fig 6A**) and by western blot, when assessing the full length  
200 PIWIL2 at the predicted molecular weight of 109 kDa and when quantified over 3 biological replicates  
201 (**Fig 6B, C**).

202

203 We then sought to assess the potential phenotypic effects of PIWIL2 depletion in these cells on cell  
204 proliferation, since increased proliferation is an indication of pro-tumorigenic behavior. To do this, we  
205 used the xCELLigence Real-Time Cell Analysis (RTCA) system, to monitor cell proliferation rates in  
206 standard 2-dimensional conditions and in real time (**Fig 6D**). Interestingly, the PIWIL2 KO cells had a  
207 significantly lower proliferation rate indicated by a slower growth curve, than the Caco2 WT control

208 cells, taking approximately twice as long for the KO cells to reach confluency at 48 hours compared to  
209 WT cells, which reached confluency in 26 hours. This shows that PIWIL2 depletion has negative effects  
210 on cell proliferation in standard 2-dimensional cultures.

211  
212 We then examined the ability of the PIWIL2 KO cells to grow in anchorage-independent conditions,  
213 which is a hallmark of pro-tumorigenic transformation. To do this, we cultured cells using a low  
214 attachment plate assay to determine if the PIWIL2 KO cells could form spheroids in these conditions  
215 (**Fig 6E-I**). Caco2 WT cells were able to form only small and very few spheroids after 10 days, which is  
216 expected since these cells are well-differentiated epithelial cells and not expected to grow in anchorage-  
217 independent conditions(Kourtidis et al., 2015). However, the PIWIL2 KO cells grew into much larger  
218 spheroids that exhibited a significantly larger area, perimeter and diameter, and were relatively  
219 symmetrical, when considering there were no significant changes in circularity. These data demonstrate  
220 that PIWIL2 KO in Caco2 cells, although results in a lower proliferation rate in 2-dimensional cultures,  
221 it promotes cell growth in an anchorage independent manner, indicating a pro-tumorigenic potential of  
222 these cells.

### 223 224 **PIWIL2 depletion increases the levels and activity of the LINE-1 transposable element**

225 Since PIWIL2 is the main enzymatic component of the PIWI pathway responsible for TE targeting and  
226 suppression, we investigated whether PIWIL2 depletion would promote TE upregulation and activation.  
227 We first examined whether LINE-1 levels were increased in the PIWIL2 KO cells by qRT-PCR of the  
228 L1RE1 RNA transcript, which includes the first ORF of the LINE-1 mRNA that encodes the ORF1p RNA  
229 binding protein required for LINE-1 retro-transposition(Beck et al., 2011, Elbarbary et al., 2016). PIWIL2  
230 depletion increased the L1RE1 transcript by 1.5-fold (**Fig 7A**), showing that LINE-1 levels are indeed  
231 upregulated. To examine whether the increased LINE-1 levels upon PIWIL2 depletion were also  
232 accompanied by increased retro-transposition activity, we utilized a retro-transposition LINE1-GFP  
233 reporter assay(Moran et al., 1996, Ostertag et al., 2000, Garcia-Perez et al., 2010, Kopera et al., 2016).  
234 In this assay, a plasmid with a full-length retro-transposition competent LINE-1 element produces GFP  
235 only when retro-transposition occurs and is an indicator of TE activity within the cell (denoted LINE1-  
236 GFP). Additionally, the assay uses a negative control plasmid with an inactive LINE-1 element that  
237 contains a defective ORF1p protein (LINE1 inactive (-)) that is unable to retro-transpose and produce  
238 GFP. Caco2 WT or PIWIL2 KO cells were transfected with either a constitutively active GFP reporter  
239 plasmid (pCEP4+) to determine transfection efficiency, the LINE1-GFP retro-transposition reporter, or  
240 the LINE1 inactive (-) plasmid as a negative control. After 48 hours, transfected Caco2 WT and PIWIL2  
241 KO cells were placed in puromycin selection for 4 days and then imaged by fluorescence microscopy  
242 to identify GFP positive cells (**Fig 7B**). The average percent of positive GFP expressing cells was

243 normalized to the transfection efficiency of each cell line for comparison (**Fig 7C**). Caco2 WT + LINE1-  
244 GFP fluorescence was minimal and not significantly different compared to Caco2 WT LINE-1 inactive  
245 (-) cells, indicating there is minimal LINE-1 activity in the Caco2 WT cells. However, PIWIL2 KO +  
246 LINE1-GFP exhibited significantly higher LINE-1 activity compared to the PIWIL2 KO + LINE1 inactive  
247 (-) cells, indicating specific LINE-1 activation in the PIWIL2 KO cells; this increased activity was also  
248 significantly higher compared to Caco2 WT + LINE1-GFP cells, demonstrating that PIWIL2 depletion  
249 not only increases LINE-1 mRNA transcript levels, but also LINE1 activity in colon epithelial Caco2  
250 cells.

### 251 252 **PIWIL2 depletion promotes DNA damage**

253 The DNA insertional activity of TEs and especially of LINE-1 elements can cause DNA damage, which  
254 is a hallmark of cancer (Gasior et al., 2006, Hanahan and Weinberg, 2011). Therefore, we examined  
255 whether the increased LINE-1 activity upon PIWIL2 depletion in Caco2 cells (**Fig 7B,C**) also results in  
256 DNA damage in these cells (**Fig 8**). Immunofluorescent staining followed by confocal microscopy of  
257 Caco2 WT and PIWIL2 KO cells for  $\gamma$ H2AX, a phosphorylated histone marker of DNA double stranded  
258 breaks(Kuo and Yang, 2008), revealed that there was a significant increase in the number of  $\gamma$ H2AX  
259 foci per cell (**Fig 8A,B**). We also confirmed increased levels of  $\gamma$ H2AX compared to total H2AX by  
260 immunoblotting (**Fig 8C**). These results demonstrate that PIWIL2 depletion in the somatic, well-  
261 differentiated colon epithelial Caco2 cells results in up regulation of transposon levels and activity, as  
262 well as in subsequent increased DNA damage, which are all promoters of pro-tumorigenic  
263 transformation. These findings, taken together with the dysregulation of the PIWI pathway and  
264 downregulation of PIWIL2 in colon tumors, as well as with the significantly increased ability of the  
265 PIWIL2 KO cells to grow in anchorage-independent conditions, underscore a tumor-suppressing role  
266 of PIWIL2 in the colon.

### 267 268 **DISCUSSION**

269 Prior studies have shown that the activation of TEs in tumors, including colon cancer, was frequent,  
270 although little is known regarding the potential mechanisms of TE activation (Pitkanen et al., 2014,  
271 Ewing et al., 2015, Solyom et al., 2012). Recently, the PIWI pathway, which is well-established to  
272 suppress transposons in the germline, has also been shown to be expressed in the soma and be  
273 implicated in cancer(Ross et al., 2014a, Siomi et al., 2011). However, reports regarding the presence  
274 of PIWI proteins in somatic tissues and the role of this pathway in tumorigenesis have been conflicting,  
275 with some supporting a tumor-suppressing and others a tumor-promoting role of the pathway. Our  
276 bioinformatic analysis, as well as our RNAseq, qRT-PCR, and protein expression data, confirm  
277 expression of PIWIL2, the key regulator of the pathway, in the colon and in the well-differentiated colon

278 epithelial Caco2 cells (**Fig. 2,3,6,Supplemental Table 1**). Our data also show that the pathway  
279 experiences significant allelic losses and its expression is downregulated in colon adenocarcinoma,  
280 with PIWIL2 having the highest percentage of deletions and allelic losses within the pathway (**Fig. 1**).  
281 Both PIWIL2 allelic losses and downregulation also correlate with poor patient survival. Furthermore,  
282 knockout of PIWIL2 in Caco2 cells resulted in increased expression and activity of the LINE-1 TE, the  
283 most abundant and only autonomous TE in humans, as well as in DNA damage and in anchorage-  
284 independent growth, all hallmarks of pro-tumorigenic transformation (**Fig 6,7,8**). Altogether, the data  
285 support the idea that PIWIL2 acts as a tumor suppressor in the colon.

286 Furthermore, when we interrogated PIWIL2 expression levels in the TCGA dataset by UALCAN  
287 analysis, PIWIL2 loss was more prevalent in the mucinous adenocarcinoma subtype of colon cancer  
288 (**Fig 3E**), which is found in 10%-20% of colon cancer patients and is characterized by  $\geq 50\%$  of the  
289 tumor volume consisting of extracellular mucins (Fleming et al., 2012, Luo et al., 2019, Huang et al.,  
290 2021). Studies have also shown that mucinous adenocarcinoma tumors exhibit a higher frequency of  
291 microsatellite instability, CpG island methylation, and lower frequency of p53 mutations (Luo et al., 2019,  
292 Huang et al., 2021). Indeed, PIWIL2 downregulation in colon tumors seems to correlate with  
293 microsatellite instability, independently of p53 status (**Fig. 3D,F**). These findings further suggest the  
294 involvement TE mobility in tumorigenesis, since retrotransposons like LINE-1 are known to give rise to  
295 de novo microsatellites during retro-transposition events due to internal proto-microsatellite sequences  
296 and poly-A mononucleotide repeats (Grandi and An, 2013). Since PIWIL2 downregulation seems to be  
297 independent of p53 status, which is key for maintaining genome integrity, it is likely that PIWIL2  
298 dysregulation in microsatellite tumors is a potential mechanism of LINE-1 activation which would be  
299 interesting to be further interrogated.

300 Our database examination also showed that PIWIL2 is downregulated in samples from patients with  
301 ulcerative colitis, which highlights a gap in current research since the PIWI pathway has not been  
302 previously studied in colitis and in inflammatory bowel disease (**Fig 5**). A few studies have indicated  
303 that there is upregulation of LINE-1 elements in inflammatory bowel disease, particularly in Crohn's  
304 Disease; however, the information on transposon expression and their regulation in these diseases is  
305 still very limited (Kanke et al., 2022, Wang et al., 2017). Given the above and that colitis and  
306 inflammatory bowel disease overall strongly predispose for colon cancer, it would be interesting to  
307 examine whether this PIWIL2 downregulation is a contributing factor to this predisposition, through  
308 upregulation of LINE elements in these diseases.

309 Interestingly, our *in vitro* studies showed that only a partial knockout of PIWIL2 is tolerated by Caco2  
310 cells, which correlates with the haploinsufficiency identified by the SWAN algorithm (**Fig 1,6A-C**). In  
311 fact, this low tolerance for PIWIL2 loss may be due to the ensuing DNA damage caused by PIWIL2

downregulation (**Fig. 8**) and may also explain their lower proliferation rates in regular 2-dimensional cultures (**Fig. 6D**). However, we found that even a 50% depletion of PIWIL2 was able to significantly promote anchorage independent growth of Caco2 cells, which are otherwise well-differentiated, and don't grow efficiently under these conditions (**Fig. 6E**). Acquisition of anchorage independent growth capability is a key event in epithelial cell pro-tumorigenic transformation. Furthermore, the increased DNA damage upon depletion of PIWIL2 was accompanied by increased levels and activity of the LINE-1 TE, indicating that TE regulation and silencing is disrupted upon PIWIL2 depletion (**Fig 7**). Both TE activation and DNA damage are driver events in tumorigenesis (Cajuso et al., 2019, Scott et al., 2016, Miki et al., 1992, Gasior et al., 2006); therefore, these findings, taken together with our current data showing early downregulation of PIWIL2 in colon tumors or even in pre-cancerous diseases, underscore a potential role of PIWIL2 in early colon tumorigenesis, which deems further investigation.

Together, the data support a tumor suppressing role for PIWIL2 in somatic cells and in colon tumorigenesis. However, PIWIL2 is part of a larger protein complex (piRISC) and the SWAN analysis identified additional members of the PIWI-piRNA pathway and of piRISC as also significantly downregulated. For example, other top targets from the SWAN analysis include the exonuclease EXD1 found in pi-bodies, the RNA helicases DDX4 and MOV10L1, PLD6, and several members of the Tudor family of proteins that are key for the functionality of piRISC. These proteins have also been identified to be dysregulated in other cancer types, mainly breast and ovarian cancers, but they have not been studied in the colonic epithelium, since this is still a novel and ongoing field of investigation (Olotu et al., 2024, Kim et al., 2014, Lee et al., 2020). Therefore, it would be of particular interest to further investigate these additional PIWI pathway components and their roles in suppressing TEs in colonic diseases. In summary, our work, through using a nuanced bioinformatic approach and by performing cell - based assays, sheds light into the currently conflicting views about the role of the PIWI pathway in somatic tissues and in cancer, opening future directions of investigation that will fully assess the tumor suppressing potential of this pathway.

## **METHODS**

### **Bioinformatic Analysis**

Multiple bioinformatic tools were used throughout this study to investigate changes in the PIWI protein pathway using data from The Cancer Genome Atlas (TCGA). The analytical tools are detailed below.

Shifted Weighted Annotation Network (SWAN): SWAN is an analytical tool used to interrogate pathway and copy-number alterations (CNAs) within the TCGA data set and can be found at the following webpage: <https://www.delaneyapps.com/>. The Single-pathway SWAN tool was used to perform Gene

346 Ontology Biological Process Analysis on the piRNA metabolic pathway in COAD with a 0.001  
347 significance threshold over 1000 permutations of the algorithm. RNA data was integrated with CNA  
348 data for this analysis and a Wilcoxon rank test was calculated as described (Bowers et al., 2022).

349  
350 cBioportal: cBioportal is another open-source web-based tool to visualize multidimensional cancer  
351 genomics data sets, including data from TCGA Pan Cancer Atlas (Cerami et al., 2012, Gao et al., 2013,  
352 de Bruijn et al., 2023). This tool can be found at the following webpage: <https://www.cbioportal.org>. The  
353 TCGA COAD data set was selected and then queried for samples with shallow deletion CNAs (loss of  
354 one allele; HETLOSS) of PIWIL2 and a plot of Overall Survival was generated using the  
355 Comparison/Survival Tool.

356  
357 UALCAN: UALCAN is a web-based tool from the University of Alabama at Birmingham that allows users  
358 to stratify TCGA data for more in-depth analysis of TCGA expression profiles. This tool can be found at  
359 the following webpage: <https://ualcan.path.uab.edu/>. A pan-cancer analysis of PIWIL2 expression was  
360 performed across multiple tumor types to compare overall expression in normal and tumor samples.  
361 PIWIL2 expression and methylation was then queried in the TCGA colon adenocarcinoma (COAD) data  
362 set and stratified by normal vs tumor, tumor stage, nodal metastasis, p53 status, histological subtype,  
363 biological sex, age, weight, and race. The median and interquartile range is displayed, and statistical  
364 significance was calculated by the UALCAN algorithm using a Welch's T-test as previously described  
365 (Chandrashekar et al., 2017, Chandrashekar et al., 2022). Results were exported from UALCAN, and  
366 graphical displays were made in Prism 10 (Graphpad).

367  
368 GEPIA2: GEPIA2 is an interactive web-based tool for analyzing RNA-seq data from the TCGA and  
369 GTEx projects that can be found at the following webpage: <http://gepia2.cancer-pku.cn/#index>. The  
370 single gene analysis search for PIWIL2 was used to plot box plots stratified by cancer subtype (MSS,  
371 MSI-L, MSI-H) of gene expression. For this study, the median expression of colon adenocarcinoma  
372 (COAD) was plotted from TCGA data available with the upper and lower quartiles. The GEPIA2  
373 program calculated statistical significance using a one-way ANOVA. A log<sub>2</sub>-fold-change of 0.5 and p-  
374 value of 0.5 were set as thresholds for the analysis (Tang et al., 2019).

375  
376 Kaplan-Meier Plotter: This web-based tool is capable of correlating mRNA expression data and survival  
377 data of colon cancer datasets from the Gene Expression Omnibus (Gyorffy, 2024). A hazard ratio with  
378 95% confidence intervals and logrank P value are calculated by the program. PIWIL2 was interrogated  
379 to determine Regression Free Survival and stratified by all tumor stages, stages 1-3 combined and

stage 4 alone. This web-based tool can be found at the following webpage <https://www.kmplot.com> (Gyorffy, 2024).

**PreMedIBD:** PreMedIBD is a web-based data mining tool for meta-analysis of ulcerative colitis tissue gene expression. This tool can be found at the following webpage: <https://premedibd.com/genes.html>. PIWIL2, PIWIL4, DDX4, PLD6, EXD1, TDRD1, TDRD9, TDRD12 and MOV10L1 were queried and the log<sub>2</sub>-Fold gene expression changes between ulcerative colitis patients and non-IBD controls were determined for each gene. The meta-analysis was calculated as previously described using a random effects model and shows the meta-log<sub>2</sub>-Fold change and 95% confidence interval (Linggi et al., 2021). A log<sub>2</sub>-fold-change of 0.5 was used as a threshold for significance. Datasets used are available in the Gene Expression Omnibus: GSE13367, GSE9452, GSE53306, GSE38713, GSE47908, GSE73661, GSE114527, GSE87466.

### **Cell Culture**

Caco2 colon epithelial cells (ATCC, #HTB-37) were cultured in MEM (Corning, #10-010-CV) with 10% fetal bovine serum (FBS) (Gibco, Fetal Bovine Serum Qualified One Shot #A31605-02), 1 mM sodium pyruvate (Gibco, #11360-070), and 1x non-essential amino-acids (NEAA) solution (Gibco, #11140-050). Cells were maintained at 37°C with 5% CO<sub>2</sub>. The Caco2 PIWIL2 knockout (KO) cell line was generated using CRISPR/Cas9 technology in collaboration with the Cell Models Core as part of the Medical University of South Carolina COBRE in Digestive and Liver Disease following the protocol by Ran et al. (Ran et al., 2013). The sgRNA sequence was designed to target exon 14 of PIWIL2 (sense: CACCGCCAATGAACTGATGCGTTGG/antisense: AAACCCAACGCATCAGTTCATTGGC) using the online Synthego tool ([www.synthego.com](http://www.synthego.com)) and synthesized by Integrated DNA Technologies, IDT. This PIWIL2-targeting sgRNA was cloned into the PX459 pSPCas9(BB)-2A-Puro vector and Caco2 cells were transfected with 30 µg the sgRNA-containing vector using Lipofectamine 3000 (Invitrogen) according to the manufacturer's protocol. After 24 hours, cells were selected with 5 µg/ml puromycin for 48 h. Successfully transfected cells were seeded to obtain single colonies, which were picked and expanded for screening by western blot and qPCR. PCR using primers designed to amplify the target region was performed (Forward1: CTCGAACACCTGGGCTCAAGCG and Reverse1: ACCACGCACAGAGGTTTCATACC and Forward2: ATCACATTCACCTTCTAAGAGA and Reverse2: GACCACGCACAGAGGTTTCAT)

### **RNA isolation, qPCR, and RNAseq of Caco2 cells**

RNA was isolated by adding 1ml of Trizol (Invitrogen # 15596018), incubating the sample at RT for 5 minutes then using the PureLink RNA mini kit (Invitrogen #12183018A) for total RNA. Final RNA

415 concentrations and purity were determined by using a NanoDrop spectrophotometer. RNA was  
416 converted to cDNA using the High Capacity cDNA Reverse Transcriptase Kit (Applied Biosystems  
417 #4368814). qPCR reactions were performed using the Taqman FAST Universal PCR master mix  
418 (Applied Biosystems #4352042), in a BioRad CFX96 Touch/Connect real time quantitative PCR  
419 machine. Data were analyzed and normalized to 18S ribosomal RNA by  $\Delta\Delta C_t$  calculations to calculate  
420 fold change compared to control samples. The Caco2 RNA sequencing that was used to extract the  
421 PIWI1-4 expression data shown in Supplemental Table 1 have been previously published and are  
422 publicly available in the GEO public database, under the accession number GSE156860(Daulagala et  
423 al., 2024).

### 425 **Immunoblotting**

426 Whole-cell protein lysates were obtained using RIPA buffer (50 mM Tris, pH 7.4, 150 mM NaCl, 1% NP-  
427 40, 0.5% deoxycholic acid, and 0.1% SDS) supplemented with protease inhibitor (RPI Research  
428 Products, #P50750-1) and phosphatase inhibitor (Thermo Fisher Scientific, Halt Phosphatase inhibitor  
429 cocktail, #1862495) at 1:100 dilution. Cell culture plates were scraped with a cell scraper, lysates were  
430 homogenized through a syringe, and then cleared by centrifugation at 15,000 rpm for 5 minutes. Protein  
431 quantification was performed using a Pierce BCA Protein Assay (Thermo Fisher Scientific, #23227).  
432 Protein extracts were mixed with Laemmli sample buffer and separated by SDS-PAGE using 4–20%  
433 Tris-Glycine eXtended (TGX) gels (Bio-Rad) and transferred to 0.2  $\mu$ m nitrocellulose membranes (Bio-  
434 Rad) with the Trans-Blot Turbo Transfer System (Bio-Rad). Transfer efficiency was determined using a  
435 Ponceau S stain (Thermo Fisher Scientific, #A40000279). Membranes were blocked in 3% milk for 45  
436 minutes and incubated overnight with primary antibody rotating at 4°C. The membranes were washed  
437 with 1x TBST, incubated with secondary antibody for 45 min at 4°C, followed by room temperature for  
438 1 hour, and then washed with 1x TBST. Signals were detected by luminescence using Pierce ECL  
439 (Thermo Fisher Scientific, #32209) and a ChemiDoc Imaging System (Bio-Rad). Blots were quantified  
440 using the Analyze gels program in FIJI/ImageJ.

### 442 **xCELLigence Proliferation Assay**

443 16 well E-plates (Agilent, # 300 600 890) were used for the experiment on an Agilent xCELLigence  
444 Real Time Cell Analysis (RTCA) Dual Purpose (DP) machine and RTCA Basic software (Agilent). Pre-  
445 warmed media was added to each well and used to take a background measurement for 1 minute.  
446 Cells were grown until 80% confluency, washed with 1xPBS, trypsinized, centrifuged at 1000 rpm for 5  
447 min and then resuspended in cell culture media for a manual cell count using trypan blue. 20,000  
448 cells/well were then plated for each cell line in a volume of 100  $\mu$ l/well for a total volume of 150  $\mu$ l/well.  
449 Each plate included blank wells with 150  $\mu$ l of media for a negative control. Cells were allowed to settle

450 and attach to the plate at room temperature in the cell culture hood for 30 minutes, after which the plate  
451 was inserted into the machine. The Xcelligence machine was set to take a measurement every hour  
452 for 48 hours. The experiment was completed with n = 3 biological replicates and 4 technical replicates  
453 per cell line. Results were exported from the RTCA software and graphical displays were made in Prism  
454 10 (Graphpad). The cell index from each run was normalized to the final end point of the Caco2 WT  
455 cell line to determine fold change and a two-way ANOVA with Greenhouse–Geisser correction and  
456 Bonferroni correction.

### 457 458 **Low Attachment (Anchorage-Independent Growth) Assay**

459 Cells were trypsinized with 0.25% Trypsin-EDTA (Gibco, #25200-056) and counted using a manual cell  
460 count and trypan blue (Corning, #25-900-CI). Cells were then suspended in culture media appropriate  
461 for the cell line that contained 2.5% basement membrane substrate (Cultrex Basement Membrane  
462 Extract, Pathclear, #3432-001-01) and plated on an ultra-low attachment 96-well plate (Corning, #3474)  
463 at a seeding density of 1000 cells per well. Plates were cultured for a total of 10 days, adding 50 ul of  
464 media to the wells every other day and were fixed using 4% paraformaldehyde (PFA) (Electron  
465 Microscopy Sciences, # 157-4) diluted to a final concentration of 1% PFA. The experiment was  
466 completed with n = 4 biological replicates and 9 technical replicates per cell line. Following fixation,  
467 plates were imaged on a Keyence BZ-X810 microscope. Images were analyzed in FIJI/ImageJ utilizing  
468 the BioVoxel Toolbox Plugin v2.6.0, thresholding and using the analyze particles function to measure  
469 the area, perimeter, Feret's diameter, and circularity of the spheroids(Brocher).

### 470 471 **LINE1 Reporter Assay**

472 The LINE1 reporter constructs used in this study were a gift from Eline Luning Prak. The plasmids used  
473 in this study contain the indicated modifications to the pCEP4 vector backbone as previously  
474 described(Moran et al., 1996, Ostertag et al., 2000, Garcia-Perez et al., 2010, Kopera et al., 2016). In  
475 detail:

476 *pCEP4puromGFP* (pCEP4+) The vector backbone is the pCEP4 plasmid with the hygromycin  
477 resistance gene replaced with puromycin for selection. It contains the coding sequence for enhanced  
478 GFP (eGFP) and constitutively expresses eGFP with puromycin selection. This is the positive control  
479 for the retrotransposition assay and is used to determine the transfection efficiency (Addgene  
480 #177922).

481 *pJM111L1eGFP (LINE1 inactive)* The vector backbone is the pCEP4 plasmid with the hygromycin  
482 resistance gene replaced with puromycin for selection. This vector contains a retro-transposition  
483 defective allele of LINE1 that contains two missense mutations (RR<sub>261-262</sub>AA) in the LINE1 ORF1-

484 encoded protein (ORF1p) and also contains the eGFP indicator cassette. This plasmid cannot express  
485 eGFP and is a negative control for the retro-transposition assay (Addgene #42941).

486 *p99LINE1RP-GFP (LINE1-GFP reporter)* The vector backbone is the pCEP4 plasmid with the  
487 hygromycin resistance gene replaced with puromycin for selection. This vector lacks the CMV promoter  
488 and contains a full-length retro-transposition competent LINE1 element and the eGFP indicator  
489 cassette subcloned into the 3'UTR of LINE1 (Addgene #42940).

490 Caco2 wild type or PIWIL2 KO cells were seeded onto 18mm circular glass coverslips in 12 well plates  
491 for immunofluorescence staining and allowed to grow until 70% confluency. Cells were transfected  
492 using Lipofectamine 3000 (Thermo Fisher #L3000-001) according to manufacturer's instructions with  
493 1µg of pCEP4puroeGFP, or 1µg pJM111L1eGFP or 1µg p99LINE1RP-GFP(Day 0). 16 hours post  
494 transfection, the media was changed with fresh cell culture media (Day 1). At 48 hours post-transfection,  
495 cells were placed in puromycin selection at a concentration of 5 µg/ml (Day 2). 48 hours later, media  
496 was changed with fresh, and cells were kept in puromycin selection (Day 4). After 4 days of puromycin  
497 selection (Day 6 post-transfection), the cells were then fixed with 4% paraformaldehyde, washed with  
498 1xPBS with 10mM glycine followed by permeabilization with 0.02% Triton-X 100 and stained with DAPI.  
499 Three fields per condition were captured and the experiment was completed with n = 4 biological  
500 replicates and imaged using a Keyence BZ-X810 microscope. Images were analyzed by FIJI/ImageJ.  
501 The average number of retro-transposition events was divided by the transfection efficiency of the  
502 pCEP4+ positive control plasmid and then normalized to the L1 inactive plasmid for each cell line.

## 503 504 **Immunofluorescence**

505 Cells were grown in 12-well plates on 18 mm circular sterile glass coverslips (Fisher Scientific #72222-  
506 01) until they reached 80% confluency. Cells were washed once with 1x PBS and fixed with 100%  
507 methanol (Thermo Fisher Scientific) at -20°C for 7 min followed by 1x PBS wash. Coverslips were then  
508 blocked with serum free Protein Block reagent (Dako, #X0909) at RT for 1hr and stained with primary  
509 antibodies diluted in Antibody Diluent (Dako, #S3022) as described in the antibodies table overnight at  
510 4°C. Cells were then washed with 1x PBS and stained with the fluorescent-labeled secondary  
511 antibodies for 1 hour at room temperature. Coverslips were then washed with 1x PBS, co-stained with  
512 DAPI (Sigma-Aldrich, #D8417) and mounted with Aqua-Poly/Mount (Polysciences, #18606-20).

## 513 514 **Confocal Imaging and Image processing**

515 Confocal images of γH2AX foci were acquired using a Leica SP8 confocal microscope with a 63x Plan-  
516 APOchromat 1.4NA DIC oil immersion objective (Leica) and 405 nm and 633 nm lasers. Image  
517 acquisition was completed using the Leica Application Suite software at 2048 × 2048 resolution and  
518 with 0.3 µm intervals along the z-axis. The same imaging parameters were used across conditions for

519 each set of experiments to allow for comparisons. Z-stacks of all samples were analyzed using the  
520 FIJI/ImageJ analysis software and a max projection of each image was used to visualize the nucleus  
521 and account for uneven cell thickness over the entire field. Three fields of each sample were captured,  
522 and the experiment was performed in n = 3 biological replicates. Total  $\gamma$ H2AX foci were quantified by  
523 thresholding the images and using the analyze particles function, then normalized to the total number  
524 of cells in the field. Nuclei on the borders were excluded from the cell count calculation in FIJI.

## 525

### 526 **Analysis and Statistics**

527 For all measurements, sample size and related statistics are indicated in the respected figure legends  
528 and were analyzed and graphed using Prism 10 (GraphPad). All experiments were performed in at  
529 least three independent experiments, unless otherwise noted, with alpha = 0.05 and representative  
530 images are shown. Statistical tests are noted in each figure legend along with p-values. For tests that  
531 required multiple comparisons, the multiplicity adjusted p-value is reported.

### 532

### 533 **ACKNOWLEDGMENTS**

534 We would like to thank Drs. Christiana Kappler and Stephen Duncan, Cell Models Core, Medical  
535 University of South Carolina Center of Biomedical Research Excellence (COBRE) in Digestive & Liver  
536 Disease (CDLD; National Institutes of Health P20 GM130457) for support with CRISPR/Cas9  
537 reagents.

### 538 **COMPETING INTERESTS**

539 No competing interests declared.

### 540 **FUNDING**

541 This work was supported by National Institute of Health grants R01 DK124553, R01 DK136658, R21  
542 CA246233, P20 GM130457 (COBRE in Digestive & Liver Disease, MUSC), P30 DK123704  
543 (Digestive Disease Research Center, MUSC), to AK; R01 GM160815 to VG; and DP2 CA280626 to  
544 JRD. A.R. was supported by National Institutes of Health training grants TL1 TR001451, UL1  
545 TR001450, T32 5T32DK124191, and 1F31DK138780-01.

547

## REFERENCES

- 548 ARIUMI, Y. 2016. Guardian of the Human Genome: Host Defense Mechanisms against LINE-1 Retrotransposition.  
549 *Front Chem*, 4, 28.
- 550 BECK, C. R., COLLIER, P., MACFARLANE, C., MALIG, M., KIDD, J. M., EICHLER, E. E., BADGE, R. M. & MORAN, J. V.  
551 2010. LINE-1 retrotransposition activity in human genomes. *Cell*, 141, 1159-70.
- 552 BECK, C. R., GARCIA-PEREZ, J. L., BADGE, R. M. & MORAN, J. V. 2011. LINE-1 elements in structural variation and  
553 disease. *Annu Rev Genomics Hum Genet*, 12, 187-215.
- 554 BERRENS, R. V., ANDREWS, S., SPENSBERGER, D., SANTOS, F., DEAN, W., GOULD, P., SHARIF, J., OLOVA, N.,  
555 CHANDRA, T., KOSEKI, H., VON MEYENN, F. & REIK, W. 2017. An endosiRNA-Based Repression Mechanism  
556 Counteracts Transposon Activation during Global DNA Demethylation in Embryonic Stem Cells. *Cell Stem*  
557 *Cell*, 21, 694-703 e7.
- 558 BOWERS, R. R., JONES, C. M., PAZ, E. A., BARROWS, J. K., ARMESON, K. E., LONG, D. T. & DELANEY, J. R. 2022.  
559 SWAN pathway-network identification of common aneuploidy-based oncogenic drivers. *Nucleic Acids Res*,  
560 50, 3673-3692.
- 561 BROCHER, J. BioVoxel Toolbox. v2.6.0 ed.
- 562 CAJUSO, T., SULO, P., TANSKANEN, T., KATAINEN, R., TAIRA, A., HANNINEN, U. A., KONDELIN, J., FORSSTROM, L.,  
563 VALIMAKI, N., AAVIKKO, M., KAASINEN, E., RISTIMAKI, A., KOSKENSALO, S., LEPISTO, A., RENKONEN-  
564 SINISALO, L., SEPPALA, T., KUOPIO, T., BOHM, J., MECKLIN, J. P., KILPIVAARA, O., PITKANEN, E., PALIN, K. &  
565 AALTONEN, L. A. 2019. Retrotransposon insertions can initiate colorectal cancer and are associated with  
566 poor survival. *Nat Commun*, 10, 4022.
- 567 CERAMI, E., GAO, J., DOGRUSOZ, U., GROSS, B. E., SUMER, S. O., AKSOY, B. A., JACOBSEN, A., BYRNE, C. J.,  
568 HEUER, M. L., LARSSON, E., ANTIPIN, Y., REVA, B., GOLDBERG, A. P., SANDER, C. & SCHULTZ, N. 2012. The  
569 cBio cancer genomics portal: an open platform for exploring multidimensional cancer genomics data.  
570 *Cancer Discov*, 2, 401-4.
- 571 CHANDRASHEKAR, D. S., BASHEL, B., BALASUBRAMANYA, S. A. H., CREIGHTON, C. J., PONCE-RODRIGUEZ, I.,  
572 CHAKRAVARTHI, B. & VARAMBALLY, S. 2017. UALCAN: A Portal for Facilitating Tumor Subgroup Gene  
573 Expression and Survival Analyses. *Neoplasia*, 19, 649-658.
- 574 CHANDRASHEKAR, D. S., KARTHIKEYAN, S. K., KORLA, P. K., PATEL, H., SHOYON, A. R., ATHAR, M., NETTO, G. J.,  
575 QIN, Z. S., KUMAR, S., MANNE, U., CREIGHTON, C. J. & VARAMBALLY, S. 2022. UALCAN: An update to the  
576 integrated cancer data analysis platform. *Neoplasia*, 25, 18-27.
- 577 DAULAGALA, A. C., CETIN, M., NAIR-MENON, J., JIMENEZ, D. W., BRIDGES, M. C., BRADSHAW, A. D., SAHIN, O. &  
578 KOURTIDIS, A. 2024. The epithelial adherens junction component PLEKHA7 regulates ECM remodeling and  
579 cell behavior through miRNA-mediated regulation of MMP1 and LOX. *bioRxiv* 10.1101/2024.05.28.596237.
- 580 DE BRUIJN, I., KUNDRU, R., MASTROGIACOMO, B., TRAN, T. N., SIKINA, L., MAZOR, T., LI, X., OCHOA, A., ZHAO, G.,  
581 LAI, B., ABESHOU, A., BAICEANU, D., CIFTCI, E., DOGRUSOZ, U., DUFILIE, A., ERKOC, Z., GARCIA LARA,  
582 E., FU, Z., GROSS, B., HAYNES, C., HEATH, A., HIGGINS, D., JAGANNATHAN, P., KALLETLA, K., KUMARI, P.,  
583 LINDSAY, J., LISMAN, A., LEENKNEGT, B., LUKASSE, P., MADELA, D., MADUPURI, R., VAN NIEROP, P.,  
584 PLANTALECH, O., QUACH, J., RESNICK, A. C., RODENBURG, S. Y. A., SATRAVADA, B. A., SCHAEFFER, F.,  
585 SHERIDAN, R., SINGH, J., SIROHI, R., SUMER, S. O., VAN HAGEN, S., WANG, A., WILSON, M., ZHANG, H.,  
586 ZHU, K., RUSK, N., BROWN, S., LAVERY, J. A., PANAGEAS, K. S., RUDOLPH, J. E., LENOUE-NEWTON, M. L.,  
587 WARNER, J. L., GUO, X., HUNTER-ZINCK, H., YU, T. V., PILAI, S., NICHOLS, C., GARDOS, S. M., PHILIP, J.,  
588 AACR PROJECT GENIE BPC CORE TEAM, A. P. G. C., KEHL, K. L., RIELY, G. J., SCHRAG, D., LEE, J.,  
589 FIANDALO, M. V., SWEENEY, S. M., PUGH, T. J., SANDER, C., CERAMI, E., GAO, J. & SCHULTZ, N. 2023.  
590 Analysis and Visualization of Longitudinal Genomic and Clinical Data from the AACR Project GENIE  
591 Biopharma Collaborative in cBioPortal. *Cancer Res*, 83, 3861-3867.
- 592 DE FAZIO, S., BARTONICEK, N., DI GIACOMO, M., ABREU-GOODGER, C., SANKAR, A., FUNAYA, C., ANTONY, C.,  
593 MOREIRA, P. N., ENRIGHT, A. J. & O'CARROLL, D. 2011. The endonuclease activity of Mili fuels piRNA  
594 amplification that silences LINE1 elements. *Nature*, 480, 259-63.
- 595 ECKSTEIN, M., JUNG, R., WEIGELT, K., SIKIC, D., STOHR, R., GEPPERT, C., AGAIMY, A., LIEB, V., HARTMANN, A.,  
596 WULLICH, B., WACH, S. & TAUBERT, H. 2018. Piwi-like 1 and -2 protein expression levels are prognostic  
597 factors for muscle invasive urothelial bladder cancer patients. *Sci Rep*, 8, 17693.

- 598 ELBARBARY, R. A., LUCAS, B. A. & MAQUAT, L. E. 2016. Retrotransposons as regulators of gene expression.  
599 *Science*, 351, aac7247.
- 600 EWING, A. D., GACITA, A., WOOD, L. D., MA, F., XING, D., KIM, M. S., MANDA, S. S., ABRIL, G., PEREIRA, G.,  
601 MAKOHON-MOORE, A., LOOIJENGA, L. H., GILLIS, A. J., HRUBAN, R. H., ANDERS, R. A., ROMANS, K. E.,  
602 PANDEY, A., IACOBUZIO-DONAHUE, C. A., VOGELSTEIN, B., KINZLER, K. W., KAZAZIAN, H. H., JR. &  
603 SOLYOM, S. 2015. Widespread somatic L1 retrotransposition occurs early during gastrointestinal cancer  
604 evolution. *Genome Res*, 25, 1536-45.
- 605 FLEMING, M., RAVULA, S., TATISHCHEV, S. F. & WANG, H. L. 2012. Colorectal carcinoma: Pathologic aspects. *J*  
606 *Gastrointest Oncol*, 3, 153-73.
- 607 FROST, R. J., HAMRA, F. K., RICHARDSON, J. A., QI, X., BASSEL-DUBY, R. & OLSON, E. N. 2010. MOV10L1 is  
608 necessary for protection of spermatocytes against retrotransposons by Piwi-interacting RNAs. *Proc Natl*  
609 *Acad Sci U S A*, 107, 11847-52.
- 610 FU, K., TIAN, S., TAN, H., WANG, C., WANG, H., WANG, M., WANG, Y., CHEN, Z., WANG, Y., YUE, Q., XU, Q., ZHANG,  
611 S., LI, H., XIE, J., LIN, M., LUO, M., CHEN, F., YE, L. & ZHENG, K. 2019. Biological and RNA regulatory  
612 function of MOV10 in mammalian germ cells. *BMC Biol*, 17, 39.
- 613 GAO, J., AKSOY, B. A., DOGRUSOZ, U., DRESDNER, G., GROSS, B., SUMER, S. O., SUN, Y., JACOBSEN, A., SINHA,  
614 R., LARSSON, E., CERAMI, E., SANDER, C. & SCHULTZ, N. 2013. Integrative analysis of complex cancer  
615 genomics and clinical profiles using the cBioPortal. *Sci Signal*, 6, pl1.
- 616 GAO, J., JING, J., SHANG, G., CHEN, C., DUAN, M., YU, W., WANG, K., LUO, J., SONG, M., CHEN, K., CHEN, C.,  
617 ZHANG, T. & DING, D. 2024. TDRD1 phase separation drives intermitochondrial cement assembly to  
618 promote piRNA biogenesis and fertility. *Dev Cell*, 59, 2704-2718 e6.
- 619 GAO, J. X. 2008. Cancer stem cells: the lessons from pre-cancerous stem cells. *J Cell Mol Med*, 12, 67-96.
- 620 GARCIA-PEREZ, J. L., MORELL, M., SCHEYS, J. O., KULPA, D. A., MORELL, S., CARTER, C. C., HAMMER, G. D.,  
621 COLLINS, K. L., O'SHEA, K. S., MENENDEZ, P. & MORAN, J. V. 2010. Epigenetic silencing of engineered L1  
622 retrotransposition events in human embryonic carcinoma cells. *Nature*, 466, 769-73.
- 623 GASIOR, S. L., WAKEMAN, T. P., XU, B. & DEININGER, P. L. 2006. The human LINE-1 retrotransposon creates DNA  
624 double-strand breaks. *J Mol Biol*, 357, 1383-93.
- 625 GORDON, I. O., AGRAWAL, N., WILLIS, E., GOLDBLUM, J. R., LOPEZ, R., ALLENDE, D., LIU, X., PATIL, D. Y., YERIAN,  
626 L., EL-KHIDER, F., FIOCCHI, C. & RIEDER, F. 2018. Fibrosis in ulcerative colitis is directly linked to severity  
627 and chronicity of mucosal inflammation. *Aliment Pharmacol Ther*, 47, 922-939.
- 628 GRANDI, F. C. & AN, W. 2013. Non-LTR retrotransposons and microsatellites: Partners in genomic variation. *Mob*  
629 *Genet Elements*, 3, e25674.
- 630 GRASSET, E., PINTO, M., DUSSAULX, E., ZWEIBAUM, A. & DESJEUX, J. F. 1984. Epithelial properties of human  
631 colonic carcinoma cell line Caco-2: electrical parameters. *Am J Physiol*, 247, C260-7.
- 632 GUIDOBONI, M., GAFA, R., VIEL, A., DOGLIONI, C., RUSSO, A., SANTINI, A., DEL TIN, L., MACRI, E., LANZA, G.,  
633 BOIOCCHI, M. & DOLCETTI, R. 2001. Microsatellite instability and high content of activated cytotoxic  
634 lymphocytes identify colon cancer patients with a favorable prognosis. *Am J Pathol*, 159, 297-304.
- 635 GYORFFY, B. 2024. Integrated analysis of public datasets for the discovery and validation of survival-associated  
636 genes in solid tumors. *Innovation (Camb)*, 5, 100625.
- 637 HAN, B. W., WANG, W., LI, C., WENG, Z. & ZAMORE, P. D. 2015. Noncoding RNA. piRNA-guided transposon  
638 cleavage initiates Zucchini-dependent, phased piRNA production. *Science*, 348, 817-21.
- 639 HANAHAN, D. & WEINBERG, R. A. 2011. Hallmarks of cancer: the next generation. *Cell*, 144, 646-74.
- 640 HANCKS, D. C. & KAZAZIAN, H. H., JR. 2016. Roles for retrotransposon insertions in human disease. *Mob DNA*, 7,  
641 9.
- 642 HE, G., CHEN, L., YE, Y., XIAO, Y., HUA, K., JARJOURA, D., NAKANO, T., BARSKY, S. H., SHEN, R. & GAO, J. X. 2010.  
643 Piwil2 expressed in various stages of cervical neoplasia is a potential complementary marker for p16. *Am J*  
644 *Transl Res*, 2, 156-69.
- 645 HIDALGO, I. J., RAUB, T. J. & BORCHARDT, R. T. 1989. Characterization of the human colon carcinoma cell line  
646 (Caco-2) as a model system for intestinal epithelial permeability. *Gastroenterology*, 96, 736-49.
- 647 HUANG, A., YANG, Y., SHI, J. Y., LI, Y. K., XU, J. X., CHENG, Y. & GU, J. 2021. Mucinous adenocarcinoma: A unique  
648 clinicopathological subtype in colorectal cancer. *World J Gastrointest Surg*, 13, 1567-1583.

- 649 IKEDA, S., TANAKA, K., OHTANI, R., KANDA, A., SOTOMARU, Y., KONO, T. & OBATA, Y. 2022. Disruption of piRNA  
650 machinery by deletion of ASZ1/GASZ results in the expression of aberrant chimeric transcripts in  
651 gonocytes. *J Reprod Dev*, 68, 125-136.
- 652 JACOBS, D. I., QIN, Q., LERRO, M. C., FU, A., DUBROW, R., CLAUS, E. B., DEWAN, A. T., WANG, G., LIN, H. & ZHU, Y.  
653 2016. PIWI-Interacting RNAs in Gliomagenesis: Evidence from Post-GWAS and Functional Analyses.  
654 *Cancer Epidemiol Biomarkers Prev*, 25, 1073-80.
- 655 JANG, H. S., SHAH, N. M., DU, A. Y., DAILEY, Z. Z., PEHRSSON, E. C., GODOY, P. M., ZHANG, D., LI, D., XING, X., KIM,  
656 S., O'DONNELL, D., GORDON, J. I. & WANG, T. 2019. Transposable elements drive widespread expression  
657 of oncogenes in human cancers. *Nat Genet*, 51, 611-617.
- 658 KANKE, M., KENNEDY NG, M. M., CONNELLY, S., SINGH, M., SCHANER, M., SHANAHAN, M. T., WOLBER, E. A.,  
659 BEASLEY, C., LIAN, G., JAIN, A., LONG, M. D., BARNES, E. L., HERFARTH, H. H., ISAACS, K. L., HANSEN, J. J.,  
660 KAPADIA, M., GUILLEM, J. G., FESCHOTTE, C., FUREY, T. S., SHEIKH, S. Z. & SETHUPATHY, P. 2022. Single-  
661 Cell Analysis Reveals Unexpected Cellular Changes and Transposon Expression Signatures in the Colonic  
662 Epithelium of Treatment-Naive Adult Crohn's Disease Patients. *Cell Mol Gastroenterol Hepatol*, 13, 1717-  
663 1740.
- 664 KIM, E. R. & CHANG, D. K. 2014. Colorectal cancer in inflammatory bowel disease: the risk, pathogenesis,  
665 prevention and diagnosis. *World J Gastroenterol*, 20, 9872-81.
- 666 KIM, K. H., KANG, Y. J., JO, J. O., OCK, M. S., MOON, S. H., SUH, D. S., YOON, M. S., PARK, E. S., JEONG, N., EO, W.  
667 K., KIM, H. Y. & CHA, H. J. 2014. DDX4 (DEAD box polypeptide 4) colocalizes with cancer stem cell marker  
668 CD133 in ovarian cancers. *Biochem Biophys Res Commun*, 447, 315-22.
- 669 KISHANI FARAHANI, R., SOLEIMANPOUR, S., GOLMOHAMMADI, M. & SOLEIMANPOUR-LICHAEI, H. R. 2023.  
670 PIWIL2 Regulates the Proliferation, Apoptosis and Colony Formation of Colorectal Cancer Cell Line. *Iran J*  
671 *Biotechnol*, 21, e3176.
- 672 KOPERA, H. C., LARSON, P. A., MOLDOVAN, J. B., RICHARDSON, S. R., LIU, Y. & MORAN, J. V. 2016. LINE-1 Cultured  
673 Cell Retrotransposition Assay. *Methods Mol Biol*, 1400, 139-56.
- 674 KOURTIDIS, A., NGOK, S. P., PULIMENO, P., FEATHERS, R. W., CARPIO, L. R., BAKER, T. R., CARR, J. M., YAN, I. K.,  
675 BORGES, S., PEREZ, E. A., STORZ, P., COPLAND, J. A., PATEL, T., THOMPSON, E. A., CITI, S. &  
676 ANASTASIADIS, P. Z. 2015. Distinct E-cadherin-based complexes regulate cell behaviour through miRNA  
677 processing or Src and p120 catenin activity. *Nat Cell Biol*, 17, 1145-57.
- 678 KU, H. Y. & LIN, H. 2014. PIWI proteins and their interactors in piRNA biogenesis, germline development and gene  
679 expression. *Natl Sci Rev*, 1, 205-218.
- 680 KUO, L. J. & YANG, L. X. 2008. Gamma-H2AX - a novel biomarker for DNA double-strand breaks. *In Vivo*, 22, 305-9.
- 681 KURAMOCHI-MIYAGAWA, S., WATANABE, T., GOTOH, K., TOTOKI, Y., TOYODA, A., IKAWA, M., ASADA, N., KOJIMA,  
682 K., YAMAGUCHI, Y., IJIRI, T. W., HATA, K., LI, E., MATSUDA, Y., KIMURA, T., OKABE, M., SAKAKI, Y., SASAKI, H.  
683 & NAKANO, T. 2008. DNA methylation of retrotransposon genes is regulated by Piwi family members MILI  
684 and MIWI2 in murine fetal testes. *Genes Dev*, 22, 908-17.
- 685 LEE, E., LOKMAN, N. A., OEHLER, M. K., RICCIARDELLI, C. & GRUTZNER, F. 2020. A Comprehensive Molecular and  
686 Clinical Analysis of the piRNA Pathway Genes in Ovarian Cancer. *Cancers (Basel)*, 13.
- 687 LEE, J. H., SCHUTTE, D., WULF, G., FUZESI, L., RADZUN, H. J., SCHWEYER, S., ENGEL, W. & NAYERNIA, K. 2006.  
688 Stem-cell protein Piwil2 is widely expressed in tumors and inhibits apoptosis through activation of  
689 Stat3/Bcl-XL pathway. *Hum Mol Genet*, 15, 201-11.
- 690 LI, Y., ZHANG, Y. & LIU, M. 2021. Knockout Gene-Based Evidence for PIWI-Interacting RNA Pathway in Mammals.  
691 *Front Cell Dev Biol*, 9, 681188.
- 692 LINGGI, B., JAIRATH, V., ZOU, G., SHACKELTON, L. M., MCGOVERN, D. P. B., SALAS, A., VERSTOCKT, B.,  
693 SILVERBERG, M. S., NAYERI, S., FEAGAN, B. G. & VANDE CASTEELE, N. 2021. Meta-analysis of gene  
694 expression disease signatures in colonic biopsy tissue from patients with ulcerative colitis. *Sci Rep*, 11,  
695 18243.
- 696 LIU, J. J., SHEN, R., CHEN, L., YE, Y., HE, G., HUA, K., JARJOURA, D., NAKANO, T., RAMESH, G. K., SHAPIRO, C. L.,  
697 BARSKY, S. H. & GAO, J. X. 2010. Piwil2 is expressed in various stages of breast cancers and has the  
698 potential to be used as a novel biomarker. *Int J Clin Exp Pathol*, 3, 328-37.
- 699 LU, Y., ZHANG, K., LI, C., YAO, Y., TAO, D., LIU, Y., ZHANG, S. & MA, Y. 2012. Piwil2 suppresses p53 by inducing  
700 phosphorylation of signal transducer and activator of transcription 3 in tumor cells. *PLoS One*, 7, e30999.

- 701 LUO, C., CEN, S., DING, G. & WU, W. 2019. Mucinous colorectal adenocarcinoma: clinical pathology and  
702 treatment options. *Cancer Commun (Lond)*, 39, 13.
- 703 MA, L., BUCHOLD, G. M., GREENBAUM, M. P., ROY, A., BURNS, K. H., ZHU, H., HAN, D. Y., HARRIS, R. A., COARFA,  
704 C., GUNARATNE, P. H., YAN, W. & MATZUK, M. M. 2009. GASZ is essential for male meiosis and suppression  
705 of retrotransposon expression in the male germline. *PLoS Genet*, 5, e1000635.
- 706 MARTINEZ, V. D., VUCIC, E. A., THU, K. L., HUBAUX, R., ENFIELD, K. S., PIKOR, L. A., BECKER-SANTOS, D. D.,  
707 BROWN, C. J., LAM, S. & LAM, W. L. 2015. Unique somatic and malignant expression patterns implicate  
708 PIWI-interacting RNAs in cancer-type specific biology. *Sci Rep*, 5, 10423.
- 709 MATHIOUDAKIS, N., PALENCIA, A., KADLEC, J., ROUND, A., TRIPSANES, K., SATTLER, M., PILLAI, R. S. & CUSACK,  
710 S. 2012. The multiple Tudor domain-containing protein TDRD1 is a molecular scaffold for mouse Piwi  
711 proteins and piRNA biogenesis factors. *RNA*, 18, 2056-72.
- 712 MESEURE, D., VACHER, S., BOUDJEMAA, S., LAE, M., NICOLAS, A., LECLERE, R., CHEMLALI, W., CHAMPENOIS,  
713 G., SCHNITZLER, A., LESAGE, L., DUBOIS, T. & BIECHE, I. 2020. Biopathological Significance of PIWI-piRNA  
714 Pathway Dereglulation in Invasive Breast Carcinomas. *Cancers (Basel)*, 12.
- 715 MIKI, Y., NISHISHO, I., HORII, A., MIYOSHI, Y., UTSUNOMIYA, J., KINZLER, K. W., VOGELSTEIN, B. & NAKAMURA, Y.  
716 1992. Disruption of the APC gene by a retrotransposal insertion of L1 sequence in a colon cancer. *Cancer  
717 Res*, 52, 643-5.
- 718 MORAN, J. V., HOLMES, S. E., NAAS, T. P., DEBERARDINIS, R. J., BOEKE, J. D. & KAZAZIAN, H. H., JR. 1996. High  
719 frequency retrotransposition in cultured mammalian cells. *Cell*, 87, 917-27.
- 720 NAM, C. H., YOUK, J., KIM, J. Y., LIM, J., PARK, J. W., OH, S. A., LEE, H. J., PARK, J. W., WON, H., LEE, Y., JEONG, S. Y.,  
721 LEE, D. S., OH, J. W., HAN, J., LEE, J., KWON, H. W., KIM, M. J. & JU, Y. S. 2023. Widespread somatic L1  
722 retrotransposition in normal colorectal epithelium. *Nature*, 617, 540-547.
- 723 NISHIMASU, H., ISHIZU, H., SAITO, K., FUKUHARA, S., KAMATANI, M. K., BONNEFOND, L., MATSUMOTO, N.,  
724 NISHIZAWA, T., NAKANAGA, K., AOKI, J., ISHITANI, R., SIOMI, H., SIOMI, M. C. & NUREKI, O. 2012. Structure  
725 and function of Zucchini endoribonuclease in piRNA biogenesis. *Nature*, 491, 284-7.
- 726 OLOTU, O., KOSKENNIEMI, A. R., MA, L., PARAMONOV, V., LAASANEN, S., LOURAMO, E., BOURGERY, M.,  
727 LEHTINIEMI, T., LAASANEN, S., RIVERO-MULLER, A., LOYTTYNIEMI, E., SAHLGREN, C., WESTERMARCK, J.,  
728 VENTELA, S., VISAKORPI, T., POUTANEN, M., VAINIO, P., MAKELA, J. A. & KOTAJA, N. 2024. Germline-  
729 specific RNA helicase DDX4 forms cytoplasmic granules in cancer cells and promotes tumor growth. *Cell  
730 Rep*, 43, 114430.
- 731 OSTERTAG, E. M., PRAK, E. T., DEBERARDINIS, R. J., MORAN, J. V. & KAZAZIAN, H. H., JR. 2000. Determination of L1  
732 retrotransposition kinetics in cultured cells. *Nucleic Acids Res*, 28, 1418-23.
- 733 PANDEY, R. R., TOKUZAWA, Y., YANG, Z., HAYASHI, E., ICHISAKA, T., KAJITA, S., ASANO, Y., KUNIEDA, T.,  
734 SACHIDANANDAM, R., CHUMA, S., YAMANAKA, S. & PILLAI, R. S. 2013. Tudor domain containing 12  
735 (TDRD12) is essential for secondary PIWI interacting RNA biogenesis in mice. *Proc Natl Acad Sci U S A*, 110,  
736 16492-7.
- 737 PENG, J. C. & LIN, H. 2013. Beyond transposons: the epigenetic and somatic functions of the Piwi-piRNA  
738 mechanism. *Curr Opin Cell Biol*, 25, 190-4.
- 739 PITKANEN, E., CAJUSO, T., KATAINEN, R., KAASINEN, E., VALIMAKI, N., PALIN, K., TAIPALE, J., AALTONEN, L. A. &  
740 KILPIVAARA, O. 2014. Frequent L1 retrotranspositions originating from TTC28 in colorectal cancer.  
741 *Oncotarget*, 5, 853-9.
- 742 RAMAT, A. & SIMONELIG, M. 2021. Functions of PIWI Proteins in Gene Regulation: New Arrows Added to the piRNA  
743 Quiver. *Trends Genet*, 37, 188-200.
- 744 RAN, F. A., HSU, P. D., WRIGHT, J., AGARWALA, V., SCOTT, D. A. & ZHANG, F. 2013. Genome engineering using the  
745 CRISPR-Cas9 system. *Nat Protoc*, 8, 2281-2308.
- 746 REUTER, M., CHUMA, S., TANAKA, T., FRANZ, T., STARK, A. & PILLAI, R. S. 2009. Loss of the Mili-interacting Tudor  
747 domain-containing protein-1 activates transposons and alters the Mili-associated small RNA profile. *Nat  
748 Struct Mol Biol*, 16, 639-46.
- 749 RODRIGUEZ-MARTIN, B., ALVAREZ, E. G., BAEZ-ORTEGA, A., ZAMORA, J., SUPEK, F., DEMEULEMEESTER, J.,  
750 SANTAMARINA, M., JU, Y. S., TEMES, J., GARCIA-SOUTO, D., DETERING, H., LI, Y., RODRIGUEZ-CASTRO, J.,  
751 DUESO-BARROSO, A., BRUZOS, A. L., DENTRO, S. C., BLANCO, M. G., CONTINO, G., ARDELJAN, D., TOJO,  
752 M., ROBERTS, N. D., ZUMALAVE, S., EDWARDS, P. A., WEISCHENFELDT, J., PUIGGROS, M., CHONG, Z.,  
753 CHEN, K., LEE, E. A., WALA, J. A., RAINE, K. M., BUTLER, A., WASZAK, S. M., NAVARRO, F. C. P.,

- 754 SCHUMACHER, S. E., MONLONG, J., MAURA, F., BOLLI, N., BOURQUE, G., GERSTEIN, M., PARK, P. J.,  
755 WEDGE, D. C., BEROUKHIM, R., TORRENTS, D., KORBEL, J. O., MARTINCORENA, I., FITZGERALD, R. C., VAN  
756 LOO, P., KAZAZIAN, H. H., BURNS, K. H., GROUP, P. S. V. W., CAMPBELL, P. J., TUBIO, J. M. C. &  
757 CONSORTIUM, P. 2020. Pan-cancer analysis of whole genomes identifies driver rearrangements promoted  
758 by LINE-1 retrotransposition. *Nat Genet*, 52, 306-319.
- 759 ROSS, R. J., WEINER, M. M. & LIN, H. 2014a. PIWI proteins and PIWI-interacting RNAs in the soma. *Nature*, 505,  
760 353-359.
- 761 ROSS, R. J., WEINER, M. M. & LIN, H. 2014b. PIWI proteins and PIWI-interacting RNAs in the soma. *Nature*, 505,  
762 353-9.
- 763 SAMBUY, Y., DE ANGELIS, I., RANALDI, G., SCARINO, M. L., STAMMATI, A. & ZUCCO, F. 2005. The Caco-2 cell line as  
764 a model of the intestinal barrier: influence of cell and culture-related factors on Caco-2 cell functional  
765 characteristics. *Cell Biol Toxicol*, 21, 1-26.
- 766 SAXE, J. P., CHEN, M., ZHAO, H. & LIN, H. 2013. Tdrkh is essential for spermatogenesis and participates in primary  
767 piRNA biogenesis in the germline. *EMBO J*, 32, 1869-85.
- 768 SCOTT, E. C., GARDNER, E. J., MASOOD, A., CHUANG, N. T., VERTINO, P. M. & DEVINE, S. E. 2016. A hot L1  
769 retrotransposon evades somatic repression and initiates human colorectal cancer. *Genome Res*, 26, 745-  
770 55.
- 771 SHI, S., YANG, Z. Z., LIU, S., YANG, F. & LIN, H. 2020. PIWIL1 promotes gastric cancer via a piRNA-independent  
772 mechanism. *Proc Natl Acad Sci U S A*, 117, 22390-22401.
- 773 SIEGEL, R. L., GIAQUINTO, A. N. & JEMAL, A. 2024. Cancer statistics, 2024. *CA Cancer J Clin*, 74, 12-49.
- 774 SIGURDSSON, M. I., SMITH, A. V., BJORNSSON, H. T. & JONSSON, J. J. 2012. The distribution of a germline  
775 methylation marker suggests a regional mechanism of LINE-1 silencing by the piRNA-PIWI system. *BMC*  
776 *Genet*, 13, 31.
- 777 SIOMI, H. & SIOMI, M. C. 2015. RNA. Phased piRNAs tackle transposons. *Science*, 348, 756-7.
- 778 SIOMI, M. C., MANNEN, T. & SIOMI, H. 2010. How does the royal family of Tudor rule the PIWI-interacting RNA  
779 pathway? *Genes Dev*, 24, 636-46.
- 780 SIOMI, M. C., SATO, K., PEZIC, D. & ARAVIN, A. A. 2011. PIWI-interacting small RNAs: the vanguard of genome  
781 defence. *Nat Rev Mol Cell Biol*, 12, 246-58.
- 782 SOLYOM, S., EWING, A. D., RAHRMANN, E. P., DOUCET, T., NELSON, H. H., BURNS, M. B., HARRIS, R. S., SIGMON,  
783 D. F., CASELLA, A., ERLANGER, B., WHEELAN, S., UPTON, K. R., SHUKLA, R., FAULKNER, G. J.,  
784 LARGAESPADA, D. A. & KAZAZIAN, H. H., JR. 2012. Extensive somatic L1 retrotransposition in colorectal  
785 tumors. *Genome Res*, 22, 2328-38.
- 786 SUN, Y. H., LEE, B. & LI, X. Z. 2022. The birth of piRNAs: how mammalian piRNAs are produced, originated, and  
787 evolved. *Mamm Genome*, 33, 293-311.
- 788 TANG, Z., KANG, B., LI, C., CHEN, T. & ZHANG, Z. 2019. GEPIA2: an enhanced web server for large-scale expression  
789 profiling and interactive analysis. *Nucleic Acids Res*, 47, W556-W560.
- 790 TUBIO, J. M., LI, Y., JU, Y. S., MARTINCORENA, I., COOKE, S. L., TOJO, M., GUNDEM, G., PIPINIKAS, C. P., ZAMORA,  
791 J., RAINE, K., MENZIES, A., ROMAN-GARCIA, P., FULLAM, A., GERSTUNG, M., SHLIEN, A., TARPEY, P. S.,  
792 PAPAEMMANUIL, E., KNAPPSKOG, S., VAN LOO, P., RAMAKRISHNA, M., DAVIES, H. R., MARSHALL, J.,  
793 WEDGE, D. C., TEAGUE, J. W., BUTLER, A. P., NIK-ZAINAL, S., ALEXANDROV, L., BEHJATI, S., YATES, L. R.,  
794 BOLLI, N., MUDIE, L., HARDY, C., MARTIN, S., MCLAREN, S., O'MEARA, S., ANDERSON, E., MADDISON, M.,  
795 GAMBLE, S., GROUP, I. B. C., GROUP, I. B. C., GROUP, I. P. C., FOSTER, C., WARREN, A. Y., WHITAKER, H.,  
796 BREWER, D., EELES, R., COOPER, C., NEAL, D., LYNCH, A. G., VISAKORPI, T., ISAACS, W. B., VAN'T VEER,  
797 L., CALDAS, C., DESMEDT, C., SOTIRIOU, C., APARICIO, S., FOEKENS, J. A., EYFJORD, J. E., LAKHANI, S. R.,  
798 THOMAS, G., MYKLEBOST, O., SPAN, P. N., BORRESEN-DALE, A. L., RICHARDSON, A. L., VAN DE VIJVER,  
799 M., VINCENT-SALOMON, A., VAN DEN EYNDEN, G. G., FLANAGAN, A. M., FUTREAL, P. A., JANES, S. M.,  
800 BOVA, G. S., STRATTON, M. R., MCDERMOTT, U. & CAMPBELL, P. J. 2014. Mobile DNA in cancer. Extensive  
801 transduction of nonrepetitive DNA mediated by L1 retrotransposition in cancer genomes. *Science*, 345,  
802 1251343.
- 803 UNHAVAITHAYA, Y., HAO, Y., BEYRET, E., YIN, H., KURAMOCHI-MIYAGAWA, S., NAKANO, T. & LIN, H. 2009. MILI, a  
804 PIWI-interacting RNA-binding protein, is required for germ line stem cell self-renewal and appears to  
805 positively regulate translation. *J Biol Chem*, 284, 6507-19.

- 806 VOUREKAS, A., ZHENG, K., FU, Q., MARAGKAKIS, M., ALEXIOU, P., MA, J., PILLAI, R. S., MOURELATOS, Z. & WANG,  
807 P. J. 2015. The RNA helicase MOV10L1 binds piRNA precursors to initiate piRNA processing. *Genes Dev*, 29,  
808 617-29.
- 809 WALTER, M., TEISSANDIER, A., PEREZ-PALACIOS, R. & BOURC'HIS, D. 2016. An epigenetic switch ensures  
810 transposon repression upon dynamic loss of DNA methylation in embryonic stem cells. *Elife*, 5.
- 811 WANG, H. L., CHEN, B. B., CAO, X. G., WANG, J., HU, X. F., MU, X. Q. & CHEN, X. B. 2015. The clinical significances  
812 of the abnormal expressions of Piwil1 and Piwil2 in colonic adenoma and adenocarcinoma. *Oncotargets*  
813 *Ther*, 8, 1259-64.
- 814 WANG, L., NORRIS, E. T. & JORDAN, I. K. 2017. Human Retrotransposon Insertion Polymorphisms Are Associated  
815 with Health and Disease via Gene Regulatory Phenotypes. *Front Microbiol*, 8, 1418.
- 816 WANG, Z. Y., GE, L. P., OUYANG, Y., JIN, X. & JIANG, Y. Z. 2024. Targeting transposable elements in cancer:  
817 developments and opportunities. *Biochim Biophys Acta Rev Cancer*, 1879, 189143.
- 818 WATANABE, T. & LIN, H. 2014. Posttranscriptional regulation of gene expression by Piwi proteins and piRNAs. *Mol*  
819 *Cell*, 56, 18-27.
- 820 WEICK, E. M. & MISKA, E. A. 2014. piRNAs: from biogenesis to function. *Development*, 141, 3458-71.
- 821 WENDA, J. M., HOMOLKA, D., YANG, Z., SPINELLI, P., SACHIDANANDAM, R., PANDEY, R. R. & PILLAI, R. S. 2017.  
822 Distinct Roles of RNA Helicases MVH and TDRD9 in PIWI Slicing-Triggered Mammalian piRNA Biogenesis  
823 and Function. *Dev Cell*, 41, 623-637 e9.
- 824 XIOL, J., CORA, E., KOGLGRUBER, R., CHUMA, S., SUBRAMANIAN, S., HOSOKAWA, M., REUTER, M., YANG, Z.,  
825 BERNINGER, P., PALENCIA, A., BENES, V., PENNINGER, J., SACHIDANANDAM, R. & PILLAI, R. S. 2012. A  
826 role for Fkbp6 and the chaperone machinery in piRNA amplification and transposon silencing. *Mol Cell*, 47,  
827 970-9.
- 828 YAN, Z., HU, H. Y., JIANG, X., MAIERHOFER, V., NEB, E., HE, L., HU, Y., HU, H., LI, N., CHEN, W. & KHAITOVICH, P.  
829 2011. Widespread expression of piRNA-like molecules in somatic tissues. *Nucleic Acids Res*, 39, 6596-607.
- 830 YANG, Z., CHEN, K. M., PANDEY, R. R., HOMOLKA, D., REUTER, M., JANEIRO, B. K., SACHIDANANDAM, R.,  
831 FAUVARQUE, M. O., MCCARTHY, A. A. & PILLAI, R. S. 2016. PIWI Slicing and EXD1 Drive Biogenesis of  
832 Nuclear piRNAs from Cytosolic Targets of the Mouse piRNA Pathway. *Mol Cell*, 61, 138-52.
- 833 ZENG, G., ZHANG, D., LIU, X., KANG, Q., FU, Y., TANG, B., GUO, W., ZHANG, Y., WEI, G. & HE, D. 2017. Co-  
834 expression of Piwil2/Piwil4 in nucleus indicates poor prognosis of hepatocellular carcinoma. *Oncotarget*, 8,  
835 4607-4617.
- 836 ZENG, Q., WAN, H., ZHAO, S., XU, H., TANG, T., OWARE, K. A. & QU, S. 2020. Role of PIWI-interacting RNAs on cell  
837 survival: Proliferation, apoptosis, and cycle. *IUBMB Life*, 72, 1870-1878.
- 838 ZHANG, X., YU, L., YE, S., XIE, J., HUANG, X., ZHENG, K. & SUN, B. 2019. MOV10L1 Binds RNA G-Quadruplex in a  
839 Structure-Specific Manner and Resolves It More Efficiently Than MOV10. *iScience*, 17, 36-48.
- 840 ZHUO, C., LI, Q., WU, Y., LI, Y., NIE, J., LI, D., PENG, J., LIAN, P., LI, B., CAI, G., LI, X. & CAI, S. 2015. LINE-1  
841 hypomethylation in normal colon mucosa is associated with poor survival in Chinese patients with  
842 sporadic colon cancer. *Oncotarget*, 6, 23820-36.

843

844

## FIGURE LEGENDS

### **Figure 1. The PIWI-piRNA pathway experiences copy number alterations (CNAs) in colon cancer.**

Shifted Weighted Annotation Network (SWAN) analysis was performed to interrogate pathway and CNAs within The Cancer Genome Atlas (TCGA) dataset. The Single-pathway SWAN tool was used to perform Gene Ontology Biological Process Analysis on the piRNA metabolic pathway in colon adenocarcinoma (COAD). A) SWAN pathway scoring for each member of the piRNA pathway where blue represents negatively scored allelic losses and red represents positively scored copy number gains within the network (Wilcoxon rank sum  $p < 1.7E-10$ ). B) Circos plot mapping allelic losses (blue) or gains (red) to each respective chromosome. C) Table of the percentages of CNAs for each member of the piRNA pathway ranked by percent biallelic deletions. D) The cBioportal database was used to interrogate TCGA COAD dataset for Overall survival of PIWIL2 allelic loss compared to unaltered tumors. Red indicates PIWIL2 shallow deletions while blue indicates samples with no CNAs. (Logrank Test  $p = 0.0204$ )

### **Figure 2. PIWIL2 is expressed in normal somatic tissues particularly of gastrointestinal origin.**

The UALCAN web-based tool was used to perform a Pan-Cancer analysis of TCGA RNA-seq data to determine PIWIL2 expression across multiple cancer types. Normal samples are indicated in blue and tumor samples are indicated in red. Tumor types queried include: bladder urothelial carcinoma (BLCA), breast invasive carcinoma (BRCA), cervical squamous cell carcinoma and endocervical adenocarcinoma (CESC), cholangiocarcinoma (CHOL), colon adenocarcinoma (COAD), esophageal carcinoma (ESCA), glioblastoma multiforme (GBM), head and neck squamous cell carcinoma (HNSC), kidney chromophobe (KICH), kidney renal clear cell carcinoma (KIRC), kidney renal papillary cell carcinoma (KIRP), liver hepatocellular carcinoma (LIHC), lung adenocarcinoma (LUAD), lung squamous cell carcinoma (LUSC), pancreatic adenocarcinoma (PAAD), prostate adenocarcinoma (PRAD), pheochromocytoma and paraganglioma (PCPG), rectum adenocarcinoma (READ), sarcoma (SARC), skin cutaneous melanoma (SKCM), thyroid carcinoma (THCA), thymoma (THYM), stomach adenocarcinoma (STAD), and uterine corpus endometrial carcinoma (UCEC).

### **Figure 3. PIWIL2 is differentially expressed in colon tumors of advanced stage and nodal metastasis, histological subtype, and age.**

PIWIL2 expression was queried in the TCGA colon adenocarcinoma (COAD) data set and stratified by comparing normal colon tissue vs A) primary tumor, B) tumor stage, C) tumor nodal metastasis, D) tumor p53 status, E) tumor histological subtype, F) tumor microsatellite stability, as well as G) age, H) weight, I) race and J) biological sex of colon cancer patients. Normal tissues were defined as adjacent non-cancerous tissue. For panels A-E and G-I the UALCAN web-based tool was used to stratify TCGA RNA-seq data for more in-depth analysis of

880 expression profiles. The median and interquartile range is displayed, and \* $p < 0.05$ , \*\* $p < 0.01$ ,  
881 \*\*\* $p < 0.001$ . For panel F The GEPIA2 tool was utilized to further stratify PIWIL2 expression in the TCGA  
882 COAD dataset by cancer subtype: micro-satellite stable (MSS), micro-satellite instable low (MSI-L), and  
883 micro-satellite instable high (MSI-H). The GEPIA2 program calculated statistical significance using one-  
884 way ANOVA (\* $p < 0.05$ ). K-L) The Kaplan-Meier Plotter tool was used to determine if PIWIL2 expression  
885 impacted patient regression free survival for all stages combined, Stages 1+2+3 and Stage 4.

886  
887 **Figure 4. The promoter of PIWIL2 is highly methylated in colon cancer.** PIWIL2 promoter  
888 methylation was queried in the TCGA colon adenocarcinoma (COAD) data set and stratified by  
889 comparing normal colon tissue vs A) primary tumor, B) tumor stage, C) tumor nodal metastasis, D)  
890 tumor p53 status, E) tumor histological subtype, as well as F) biological sex, G) age, H) weight, and I)  
891 race of colon cancer patients. Normal tissues were defined as adjacent non-cancerous tissue. The  
892 median and interquartile range is displayed, and \* $p < 0.05$ , \*\* $p < 0.01$ , \*\*\* $p < 0.001$ . A beta value closer to  
893 1 indicates higher levels of methylation.

894  
895 **Figure 5. PIWIL2 is downregulated in ulcerative colitis patients compared to healthy, non-IBD**  
896 **patients.** A meta-analysis of ulcerative colitis tissue gene expression was performed using the  
897 PreMedIBD Gene Tool. A) PIWIL2, B) PIWIL4, C) MOV10L1, D) TDRD1, E) TDRD9, F) TDRD12, G)  
898 DDX4, H) PLD6 and I) EXD1 were queried and the  $\log_2$ -fold gene expression changes between  
899 ulcerative colitis patients and non-IBD controls were determined for each gene. The meta-analysis was  
900 calculated using a random effects model and shows the meta- $\log_2$ -Fold change and 95% confidence  
901 interval. Ulcerative Colitis datasets used are available in the Gene Expression Omnibus: GSE13367,  
902 GSE9452, GSE53306, GSE38713, GSE47908, GSE73661, GSE114527, GSE87466 and are  
903 represented by grey dots. The summary fold change is displayed with a blue line indicating  
904 downregulation, while a positive line indicates upregulation. A  $\log_2$ -fold-change of 0.5 was used as a  
905 threshold for significance.

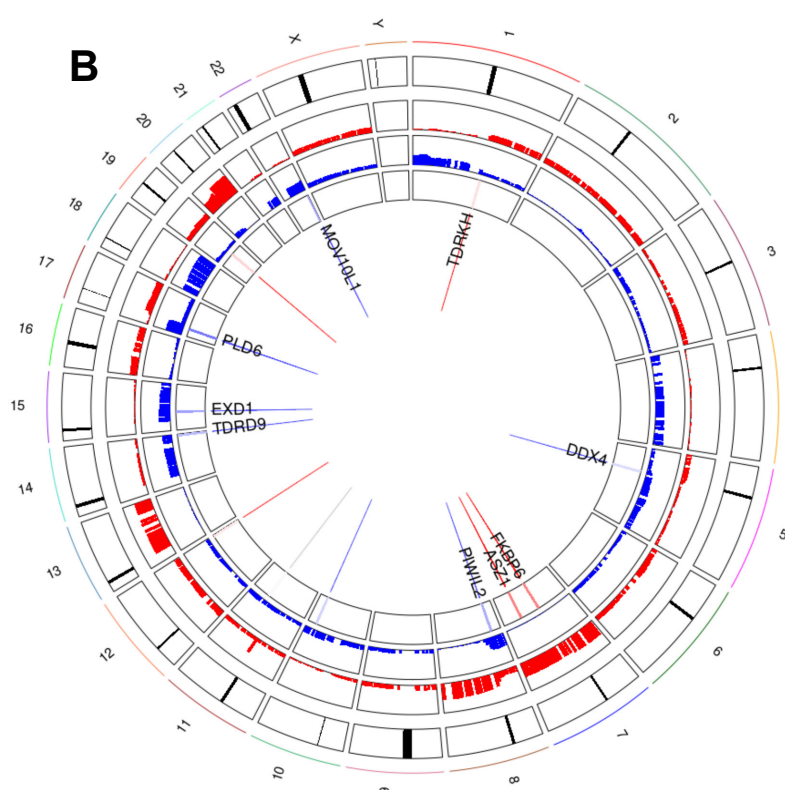
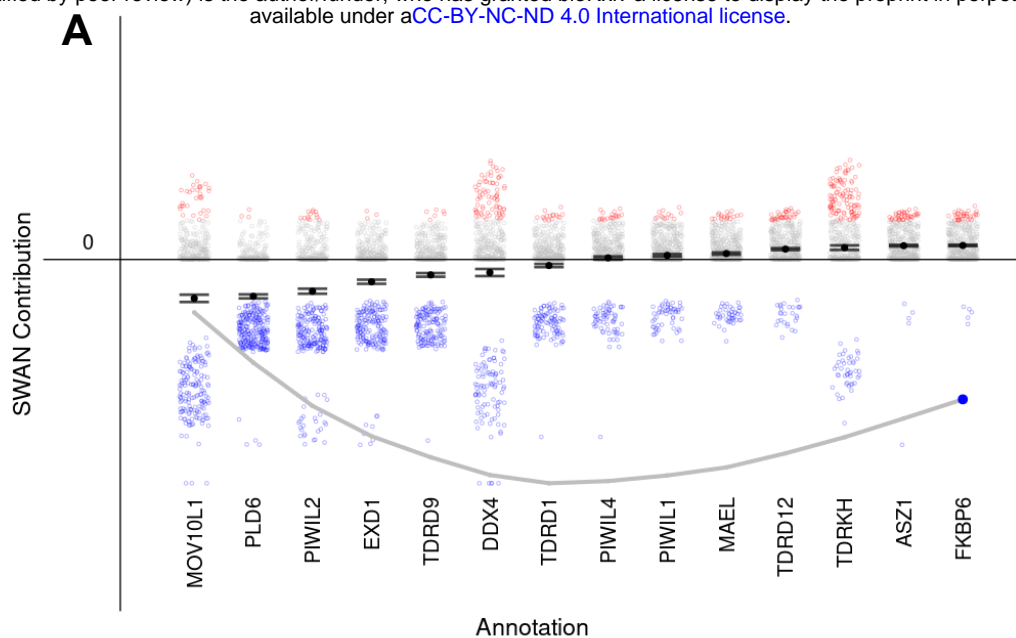
906  
907 **Figure 6. The characterization of PIWIL2 CRISPR KO cells reveals increased spheroid growth**  
908 **compared to wild type Caco2 cells.** A) qPCR of PIWIL2 comparing PIWIL2 KO to Caco2 wild type  
909 (WT). Data were analyzed and normalized to 18S ribosomal RNA by  $\Delta\Delta Ct$  calculations to calculate fold  
910 change. (n=3 biological replicates, mean  $\pm$  SE, t-test \* $p = 0.0309$ ). B) Representative western blot of  
911 total PIWIL2 and  $\beta$ -actin (Actin) loading control in Caco2 WT and PIWIL2 KO cells. Two bands are  
912 visible at the expected molecular weight of full length PIWIL2 of 109 kDa. C) Quantification of the upper  
913 band of PIWIL2 by western blot to confirm the knockout (n=3 biological replicates, mean  $\pm$  SE, t-test  
914 \*\* $p = 0.0025$ ). D) xCELLigence cellular impedance assay to examine the proliferation rates of Caco2

915 WT and PIWIL2 KO cells in 2-dimensions (2D) (n=3 biological replicates, two-way ANOVA with Geisser-  
916 Greenhouse correction and Bonferroni correction for multiple comparisons, Time x Cell Line  
917 \*\*\*\*p<0.0001). E) Representative Images of Caco2 WT and PIWIL2 KO cells grown in anchorage  
918 independent conditions. F) Area of Caco2 WT and PIWIL2 KO spheroids (\*\*p=0.0001) G) Perimeter  
919 of Caco2 WT and PIWIL2 KO spheroids (\*\*p=0.0008) H) Diameter of Caco2 WT and PIWIL2 KO  
920 spheroids (\*\*p=0.0005) I) Circularity of Caco2 WT and PIWIL2 KO spheroids (p=0.5041). For the low  
921 attachment assay n=4 biological replicates, mean  $\pm$  SE is displayed, t-test was used for statistical  
922 analysis between groups.

923  
924 **Figure 7. PIWIL2 depletion increases LINE1 levels and activity.** A) qPCR of L1RE1 comparing  
925 PIWIL2 KO to Caco2 WT. Data were analyzed and normalized to 18S ribosomal RNA by  $\Delta\Delta C_t$   
926 calculations to calculate fold change. (n=3 biological replicates, mean  $\pm$  SE, t-test \*p = 0.0267) B)  
927 Representative fluorescent images of Caco2 WT or PIWIL2 KO cells that were transfected with either  
928 a constitutively active GFP reporter (pCEP4+), a LINE1 retro-transposition defective reporter (LINE1  
929 inactive (-)) or a LINE1-GFP reporter plasmid that expresses GFP only when LINE1 retro-transposition  
930 occurs. C) Quantification of the average % positive GFP expressing cells normalized to transfection  
931 efficiency for each cell line. (n = 4 biological replicates with 3 fields taken per condition and averaged,  
932 mean  $\pm$  SE, two-way ANOVA with Bonferroni correction for multiple comparisons, PIWIL2 KO LINE1  
933 inactive (-) vs. PIWIL2 KO LINE1 GFP \*p = 0.0212, Caco2 WT LINE1 inactive (-) vs. PIWIL2 KO  
934 LINE1 GFP \*\*p = 0.0076, Caco2 WT LINE1 GFP vs. PIWIL2 KO LINE1 GFP \*\*p = 0.0091).

935  
936 **Figure 8. PIWIL2 depletion promotes DNA damage.** A)  $\gamma$ H2AX increases in PIWIL2 KO cells  
937 compared to Caco2 WT cells by immunofluorescence. Representative confocal images shown B)  
938 Quantification of  $\gamma$ H2AX foci per cell (n = 9 fields (3 biological replicates, 3 fields per replicate), mean  
939  $\pm$  SE, t-test \*p = 0.0151) C) Representative western blot of total H2AX, phosphorylated  $\gamma$ H2AX, and  $\beta$ -  
940 actin (Actin) loading control in Caco2 and PIWIL2 KO cells.

941  
942 **Supplemental Table 1. PIWI mRNAs in Caco2 cells.** PIWIL2 and PIWIL4 are expressed in Caco2  
943 cells. Gene symbol, gene ID and average reads per million (avg rpms) are displayed. n=3 biological  
944 replicates.



**C**

Gene	Percent Deleted	Percent Allelic Loss	Percent Normal	Percent Extra Allele	Percent Amplified
PIWIL2	5.9	38.8	37	18.3	0
EXD1	1.8	36.6	58	3.6	0
DDX4	1.1	20.5	69.3	8.8	0.2
PLD6	0.9	54	42	3.2	0
MOV10L1	0.7	35.7	60.7	2.9	0
ASZ1	0.2	0.9	49.2	49.2	0.5
PIWIL4	0.2	14.2	72.9	12.4	0.2
TDRD1	0.2	21.9	72.9	4.7	0.2
TDRD9	0.2	32.3	60.3	7.2	0
FKBP6	0	1.1	49.7	49	0.2
MAEL	0	9.7	68.8	21	0.5
PIWIL1	0	12.2	68.4	19	0.5
TDRD12	0	6.1	73.4	19.4	1.1
TDRKH	0	9.9	70	19.6	0.5

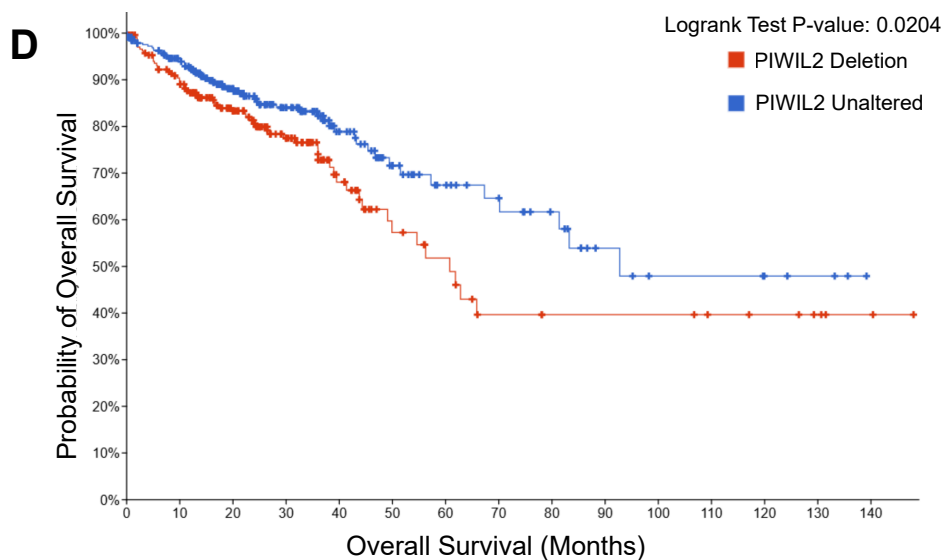


Figure 1

Expression of PIWIL2 across TCGA cancers (with tumor and normal samples)

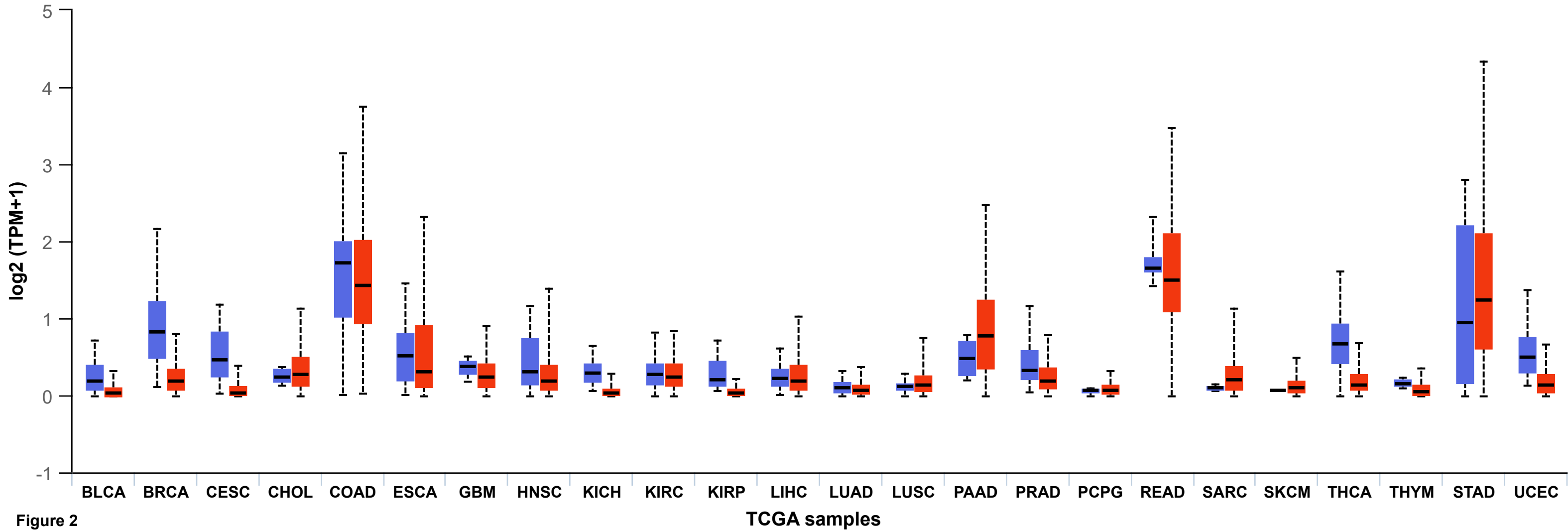
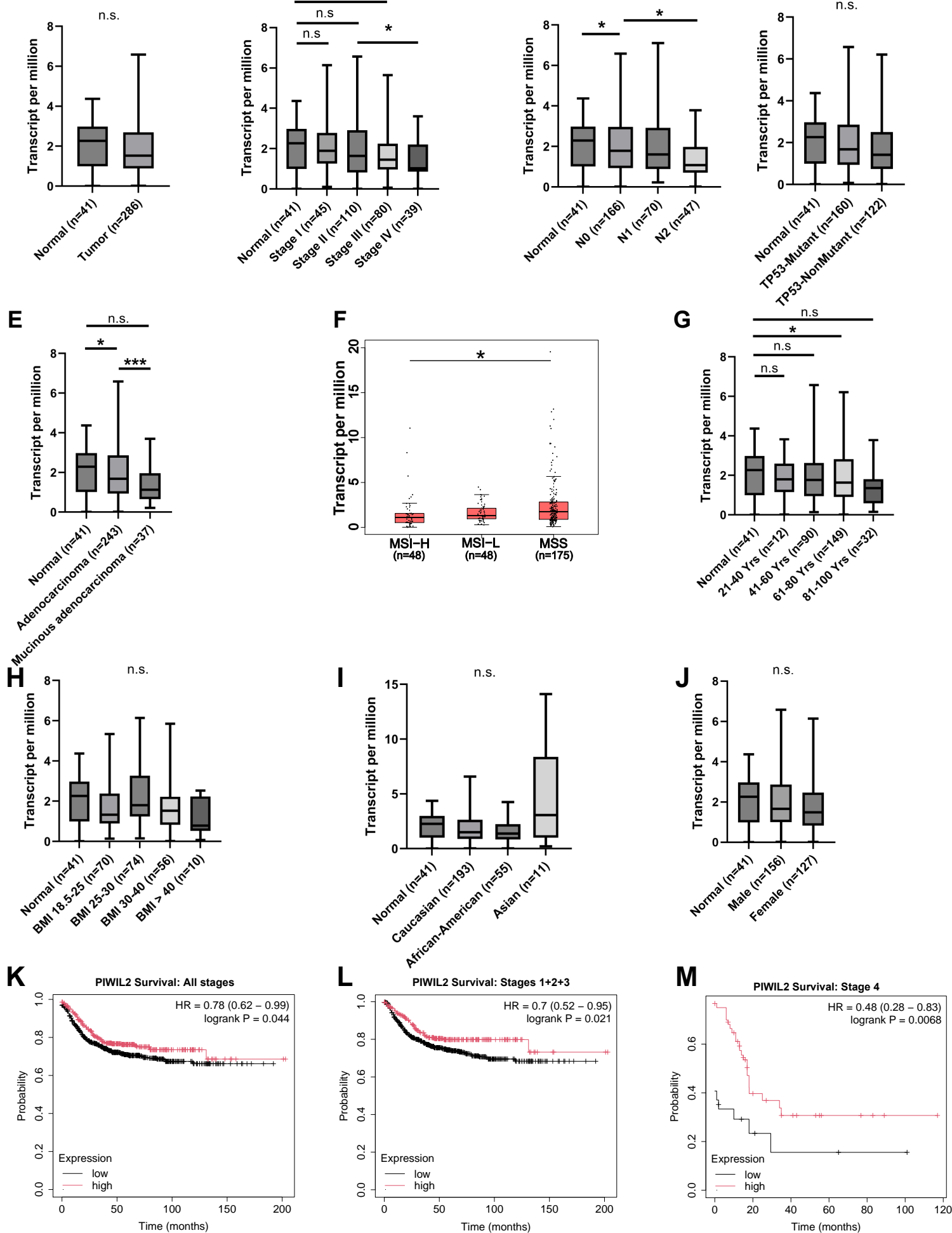


Figure 2



**Figure 3**

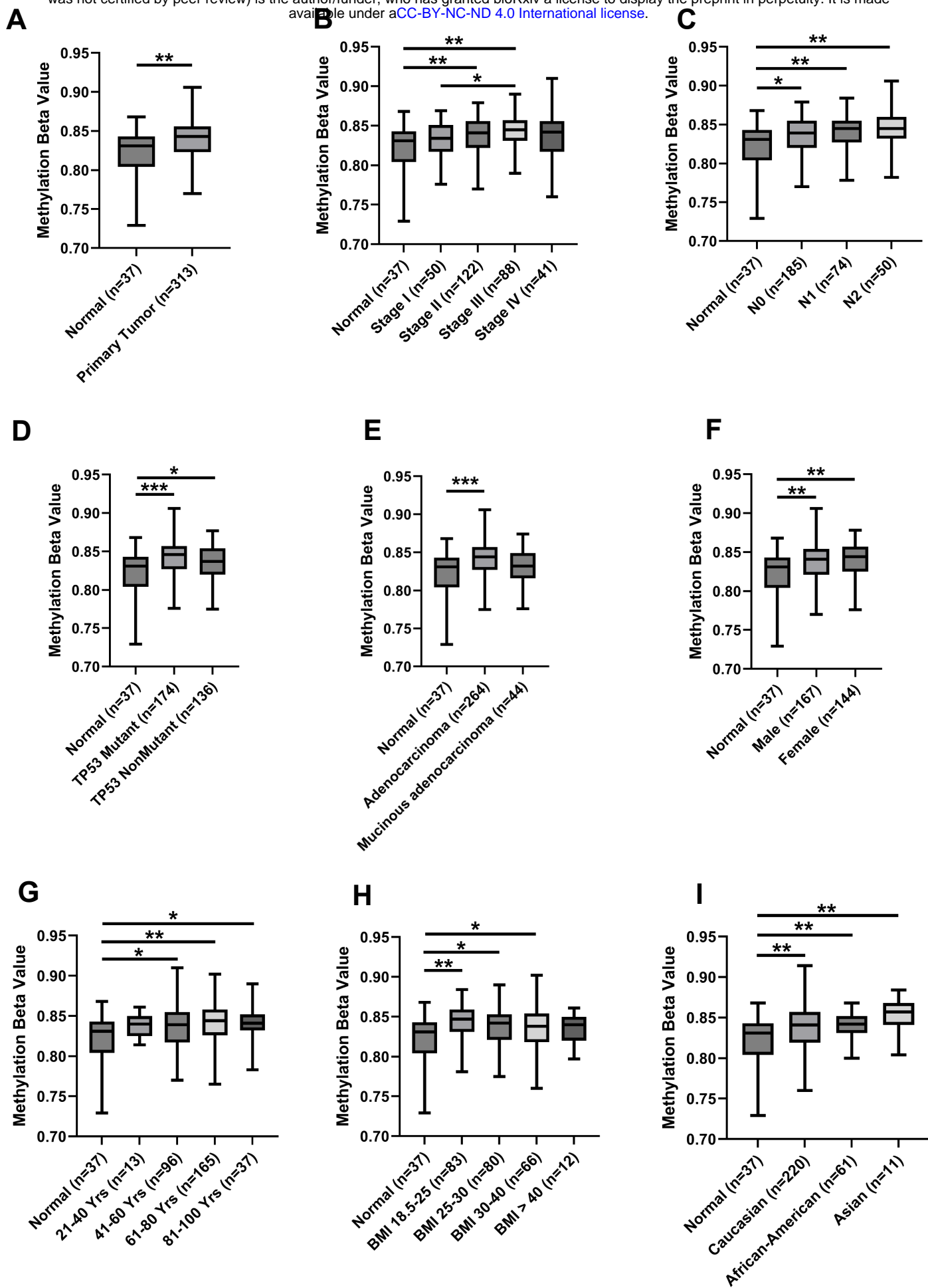
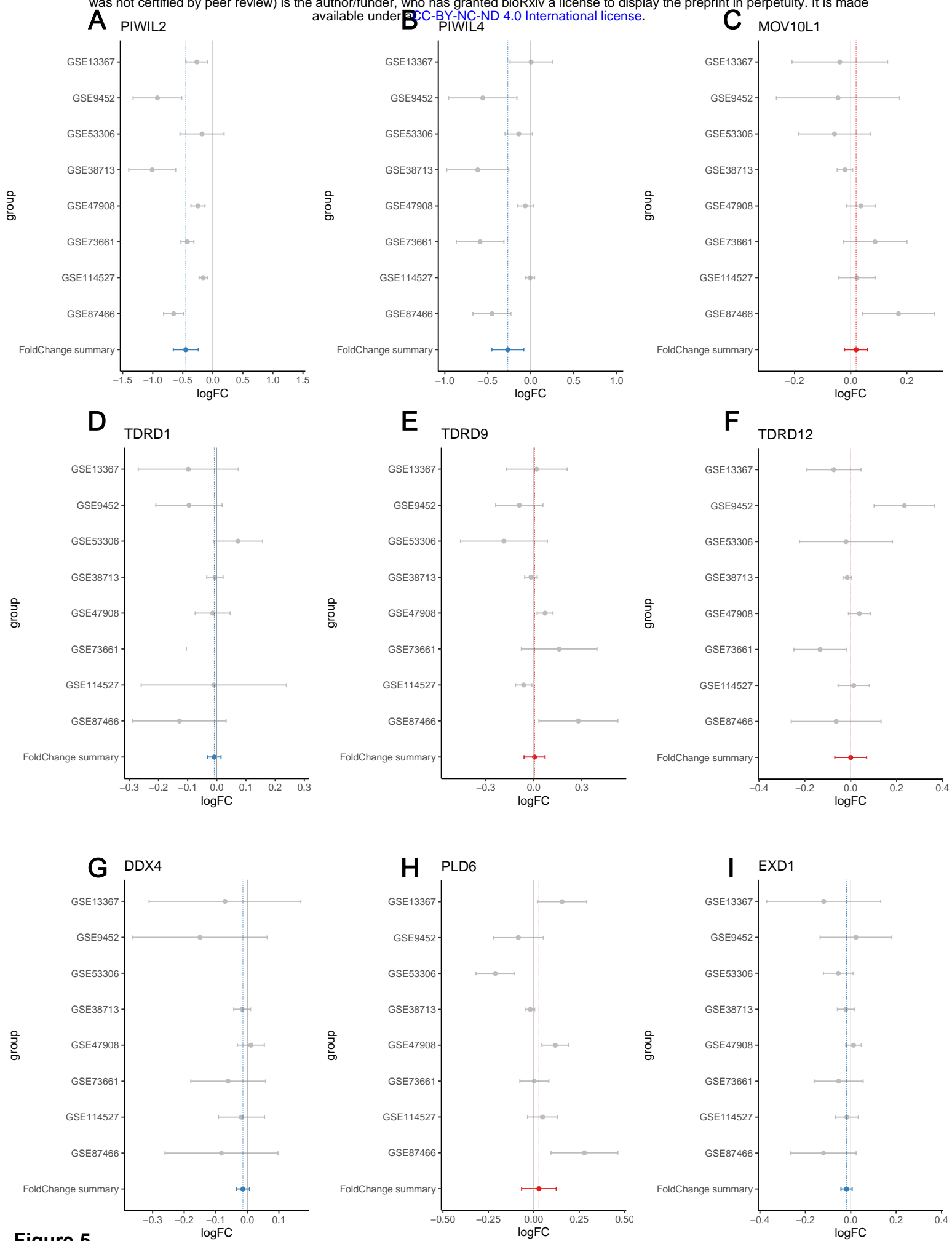


Figure 4



**Figure 5**

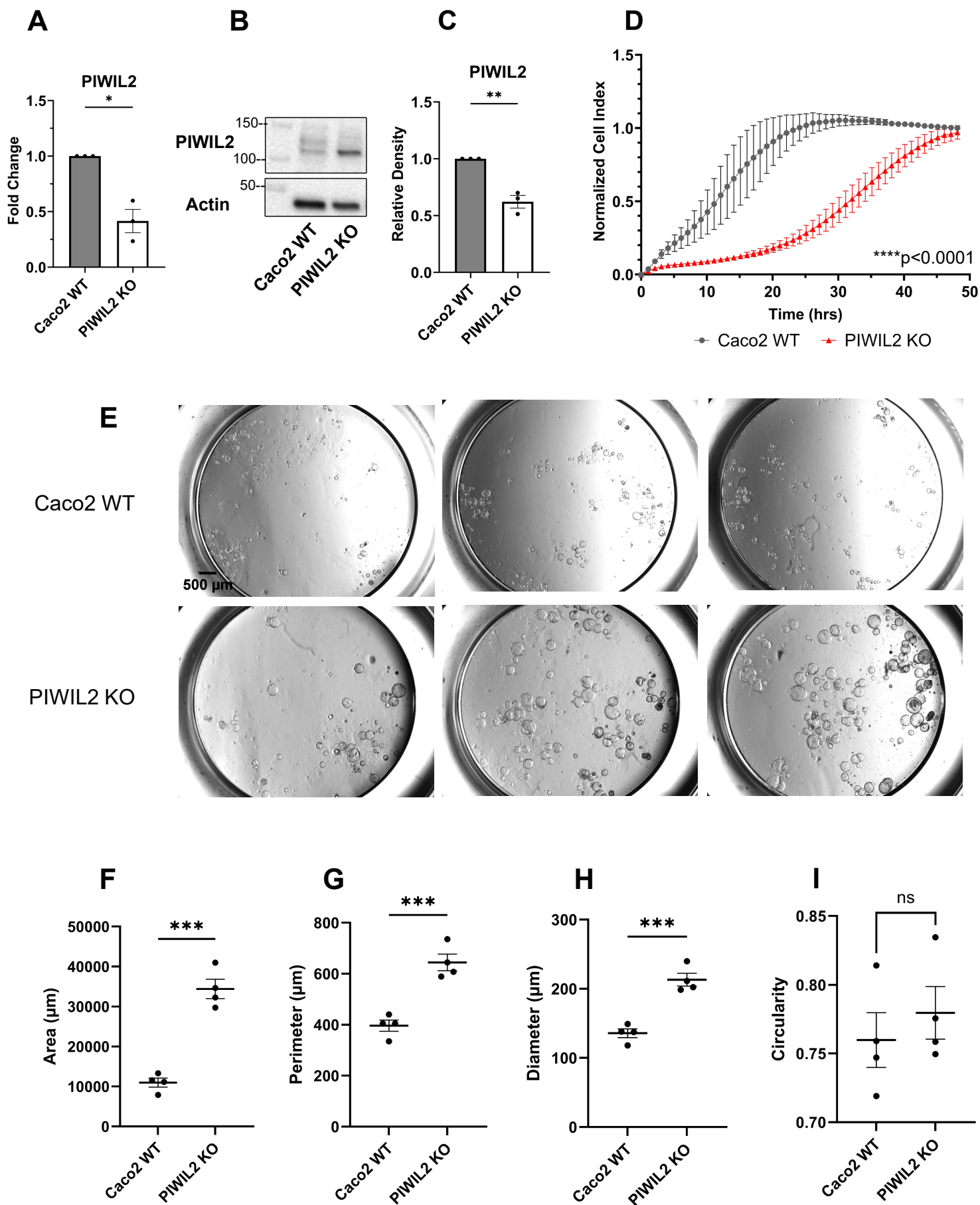


Figure 6

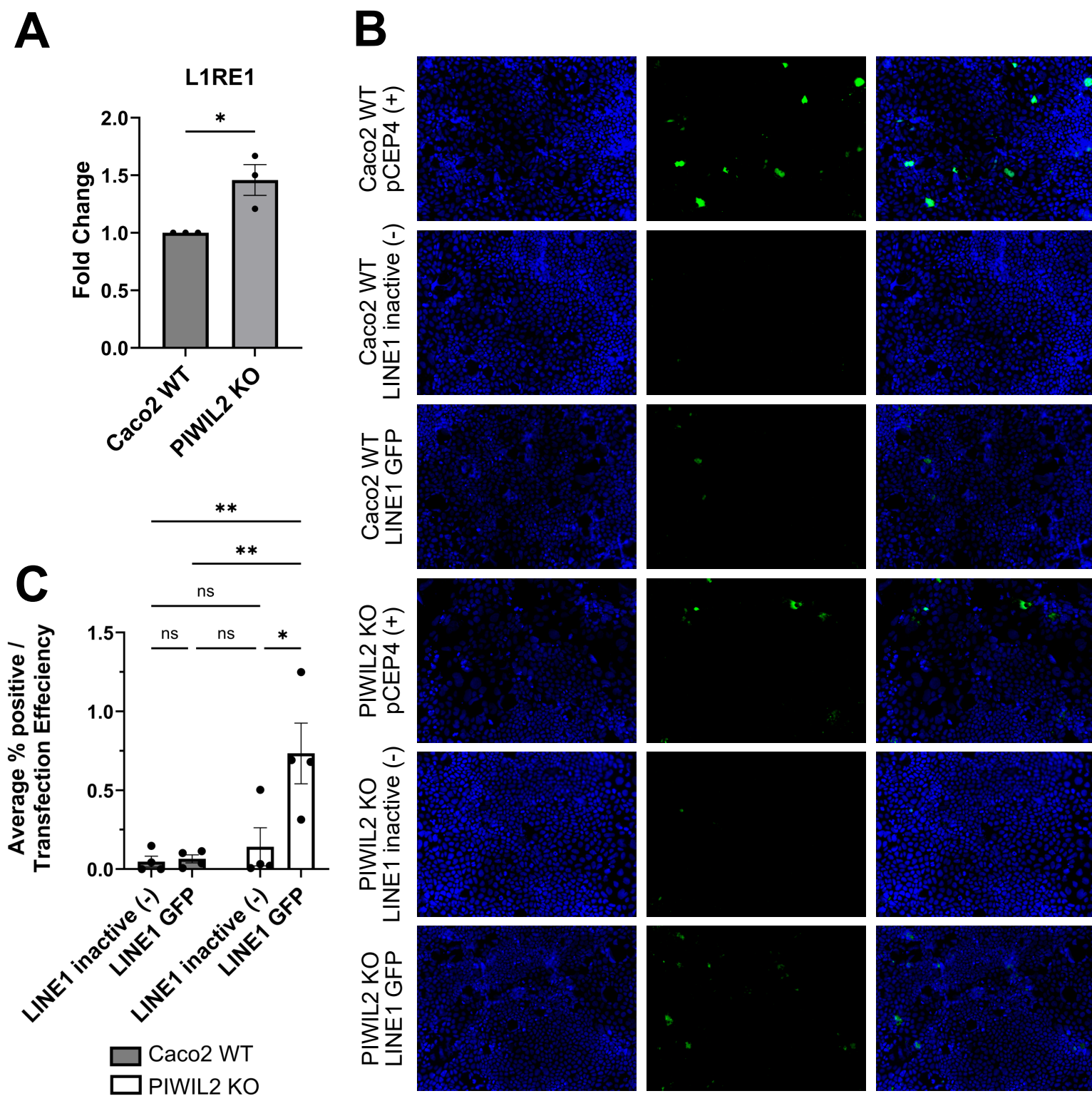


Figure 7

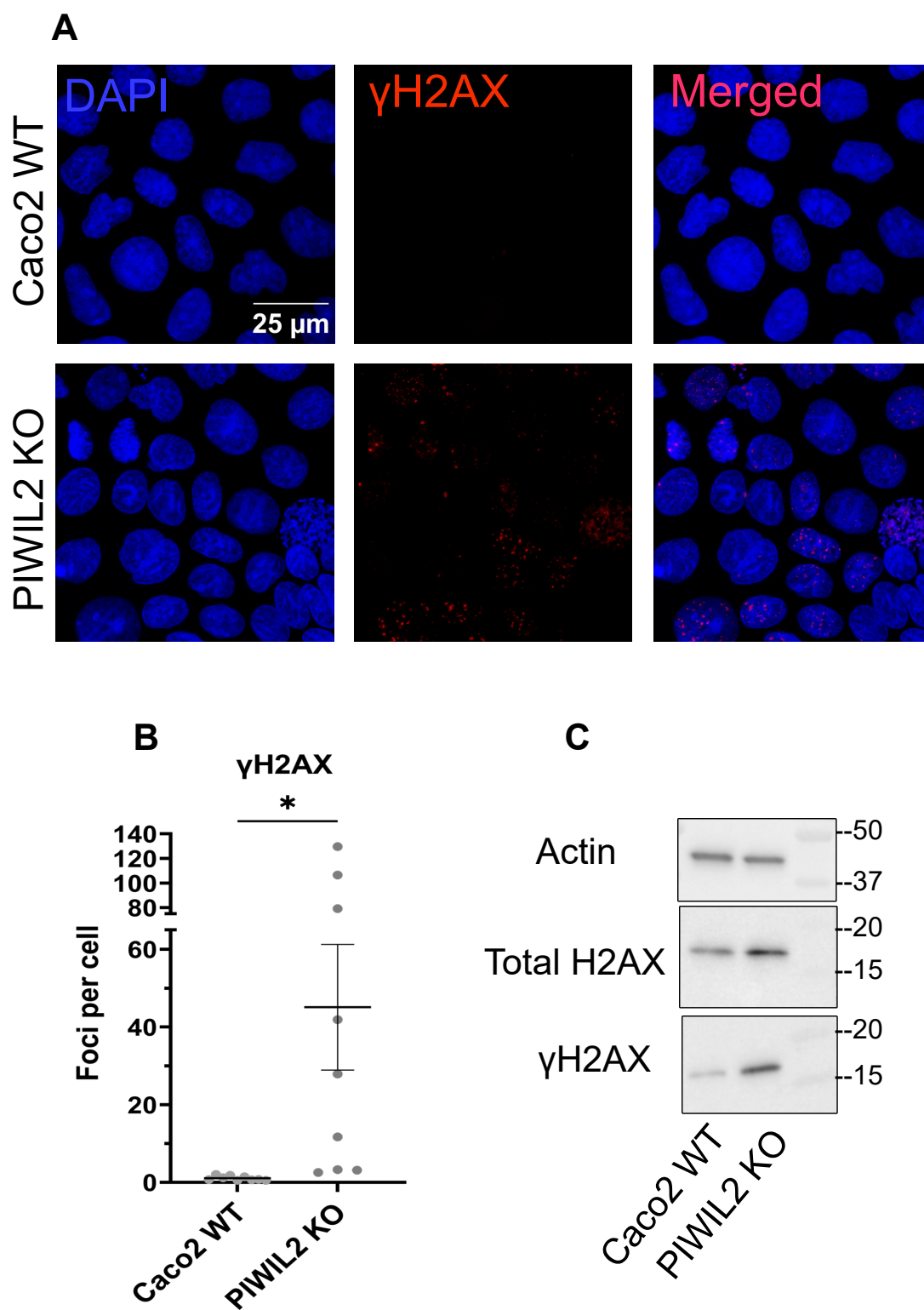


Figure 8

<b>Table 1. PIWI mRNAs in Caco2 cells</b>		
<b>Symbol</b>	<b>GeneID</b>	<b>avg rpms*</b>
PIWIL1	9271	0.0
PIWIL2	55124	94.7
PIWIL3	440822	19.7
PIWIL4	143689	261.3
*avg reads/million; 3 biological replicates		

**Supplemental Table 1**

## SUPPLEMENTAL MATERIALS

### Antibodies

#### Primary Antibodies

Antibody Name	Company	Catalogue Number	Animal	WB dilution	IF dilution
PIWIL2	Sigma Aldrich	SAB3500749	Rb	1 to 1000	-
$\beta$ -actin (Actin)	Cell Signaling	4967L	Rb	1 to 2000	-
H2AX total	Santa Cruz	sc517336	Ms	1 to 1000	-
$\gamma$ H2AX	Cell Signaling	20 E3 (9718T)	Rb	1 to 1000	1 to 400 (MeOH Fixed)

#### Secondary Antibodies

Antibody Name	Company	Catalogue Number	Animal	WB dilution	IF dilution
HRP-anti-rabbit	Jackson ImmunoResearch	711-035-152	Rb	1 to 2000	-
HRP-anti-mouse	Jackson ImmunoResearch	715-035-150	Ms	1 to 2000	-
Alexafluor 647 anti-mouse	Invitrogen	A21236	Ms	-	1 to 500 (MeOH Fixed)

#### qPCR Probes

Probe name	Company	Assay ID
18S	Thermo Fisher	Hs99999901_s1
PIWIL2	Thermo Fisher	Hs01032719_m1
L1RE1(APFVNJ2)	Thermo Fisher	custom sequence